Master thesis

Name:	Andrés Ramírez Sánchez
Matr.-Nr.:	426477

Theme:	Simulation of heat distribution during frictional contact between polycrystalline cubic boron nitride and diamond

Supervisor Assistant:	Ulrich Müller, M.Sc. RWTH
Place:	Aachen
Date:	02.11.2021

This work was presented at the Laboratory for Machine Tools and Production Engineering (WZL), Chair of Manufacturing Technology.

Aachen, 10th of May 2021
U. Müller - Tel. 28188

Master Thesis

for Mr. Cand. -M.Sc. Andrés Ramírez Sánchez

Matriculation number: 426477

Topic: *Simulation of heat distribution during frictional contact between polycrystalline cubic boron nitride and diamond*

In the automotive and aerospace industries, machining processes are constantly optimized to increase efficiency. In addition, these industries are in increasing demand of hard-to-machine materials such as nickel- and titanium-based-superalloys. Hence, a trend towards the use of superhard cutting materials such as polycrystalline cubic boron nitride (pcBN) and polycrystalline diamond (PCD) is observed. pcBN is applicable for the machining of ferrous alloys due to the high chemical and thermal stability of pcBN, whereas PCD is not applicable in this case due to its chemical affinity to ferrous. A disadvantage of using pcBN as a cutting material are the higher costs compared to conventional cutting materials such as cemented carbides and high-speed steels. In particular, the grinding process accounts for up to 30 % of the manufacturing costs of pcBN cutting tools. This is mainly due to high grinding wheel wear and low material removal rates. Therefore, grinding on the basis of knowledge-based process design offers great potential for reducing manufacturing costs.

Since friction is an essential driver of grinding wheel wear, this phenome has to be researched more in detail during grinding of pcBN in order to enable a knowledge-based process design. Friction is a phenome of the tribological system in the contact zone A_W between the abrasive diamond grain and the PCBN workpiece material. Due to the small scale of the contact zone, the measurement of the tribological state variables such as the contact temperature is prone to errors. Hence, a numerical simulation has to be developed in order to analyze the heat distribution in the contact zone A_W based on a frictional contact approach.

The scope of this work is to develop a numerical simulation of the generation of heat in the contact zone A_W between diamond abrasive grains and the pcBN workpiece material. For this purpose, an existing simulation model for the calculation of heat during frictional contact between diamond abrasive grains and PCD as workpiece material will be adapted and evaluated. The adaption includes the material properties and microstructure of pcBN, the consideration of ambient air as well as lubricant. Subsequently, the temperature in the workpiece material and the diamond abrasive grains is evaluated for different input parameters based on a systematic design of experiments. Finally, the results, limitations and conclusions will be explained and discussed.

In detail, the following subtasks have to be solved:

- Literature research regarding pcBN material, grinding of pcBN and numerical simulation of frictional as well as abrasive contact
- Adaption of an existing FEM simulation model in Abaqus
- Conduction of simulations based on a systematic design of experiments
- Analysis and evaluation of results obtained by the simulation
- Documentation of the work in scientific manner

Prof. Dr.-Ing. Thomas Bergs

I Table of contents

II Formulas and Abbreviations

Symbol	Unit	Description
A_{cu}	mm^2	Chip cross sectional area
A_t	-	Amplitude value
A_w	mm^2	Contact zone between workpiece and grinding wheel
a_e	µm	Depth of cut
b_s	mm	Grinding wheel width
$b_{s,eff}$	mm	Effective grinding wheel width
b_w	mm	Workpiece width
C	W/K	Heat capacity
c_p	J/kg·K	Specific heat capacity at constant pressure
d_g	µm	c-BN grain size diameter
d_p	µm	Pyrometer diameter
d_{Qt}	%	Disturbance
d_s	mm	Grinding wheel diameter
d_w	mm	Workpiece diameter
E	GPa	Young Modulus
e_c	J/mm^3	Specific grinding energy
F^T	N	Cutting forces vector
F_a	N	Axial force
F_c	N	Cutting force
F_f	N	Feed force
F'_n	N/mm^2	Specific normal force
F_n	N	Normal force

Symbol	Unit	Description
F_t	N	Tangential force
F_{th}	N	Thrust force
f	mm/rev	Feed speed
G	MPa	Shear modulus
HFL	W/mm^2	Heat flux load
HR	-	Nonlinear system matrix regression
H_V	GPa	Hardness
h_{cu}	µm	Chip thickness
$h_{cu,crit}$	µm	Critical chip thickness
h_{kss}	W/m^2·K	Heat transfer factor of cooling lubricant
h_{Qt}	Grains	Horizontal number of grains
h_t	cm	Height of pyramid
K	-	Constant for regression analysis
K_{Ic}	Mpa·m$^{0.5}$	Fracture toughness
k_{kss}	-	Cooling lubricant factor
k_{sls}	-	Grinding wheel specification factor
l_g	mm	Geometrical contact length
l_{mesh}	µm	Mesh element length
l_w	mm	Workpiece length
M	-	Membership value
N_{kin}	mm^{-2}	Kinematic cutting-edge number per surface
n_w	s^{-1}	number of workpiece revolutions
o_{Qt}	-	Offset

Symbol	Unit	Description
P'_c	W/mm^2	Specific grinding power
P_c	W	Grinding power
p	GPa	Pressure
Q'_w	mm^3/s	Specific material removal rate
Q_w	mm^3/s	Material removal rate
q_g	W/mm^2	Heat flow introduced by the grain
q_{kss}	W/mm^2	Heat flow via cooling lubricant
q_s	W/mm^2	Heat flow via grinding wheel
q_{sp}	W/mm^2	Heat flow via chips
q_t	W/mm^2	Total heat flow
q_w	W/mm^2	Heat flow via workpiece
R_i	-	Heat transfer factor
r_g	mm	Contact radius grit/workpiece
s_{Qt}	-	Spacing
T	°C	Temperature
T_{DBW85}	°C	Maximum temperature in the contact zone of the pcBN DBW85 workpiece
T_{WP}	°C	Maximum temperature in the contact zone of the workpiece
T_μ	mm	Grain cutting depth
t	s	Time
VB	mm	Flank wear
VN	mm	Notch wear
VS	mm	Nose wear
v_c	m/s	Cutting Speed
v_{Qt}	Grains	Vertical number of grains

Symbol	Unit	Description
v_s	m/s	Grinding wheel circumferential speed
v_w	m/min	Workpiece feed rate
w	%	Fraction of content
x^T	-	Operation variables vector
Greek symbols		
α	K^{-1}	Thermal expansion
β_n	-	Regression coefficients
$\dot{I}$	µm/h	Deposition rate
Δl_w	mm	Reduction of workpiece length
$\dot{\varepsilon}$	mm/s	Deformation rate
ε	-	Random regression error
λ	W/m·K	Thermal conductivity
μ	-	Coefficient of friction
v	-	Poisson ratio
ρ	kg/m^3	Density
π	-	Constant
τ_o	MPa	Initial stress
σ	MPa	Stress

Abbreviations	Description
Ag	Silver
Al	Aluminum
Al_2O_3	Aluminum oxide (corundum)
AlCrN	Aluminum chromium nitride
ANN	Artificial neural network
bcBN	Binderless Polycrystalline cubic boron nitride
BCC	Body centered cubic
BH	High content of cBN
BL	Low content of cBN
cBN	Cubic crystalline boron nitride
CEL	Coupled Eulerian-Lagrangian
CFRP	Carbon fiber reinforced plastics
Co	Cobalt
CVD	Chemical Vapor Deposition
DD	Polycrystalline diamond without binder
DIN	Deutsches Institut für Normung e.V.
DP	Polycrystalline diamond with binder
e.g.	exampli gratia (for example)
ECR	Electron-Cyclotron-Resonance
et al.	Et alii/aliae (and others)
FCC	Face centered cubic
FEA	Finite element analysis
FEM	Finite element method
FL	Fuzzy logic
HCP	Hexagonal closed packed

Abbreviations	Description
HFCVD	Hot filament chemical vapor deposition
HPHT	High pressure high temperature
HV	Vickers Pyramid Number
i.e.	id est (that is)
MCD	Monocrystalline diamond
MD	Molecular dynamics
MF	Membership function
MMC	Metal matrix composites
Ni	Nickel
NN	Neural network
NTM	Nanostructured materials
Pb	Lead
pcBN	Polycrystalline cubic boron nitride
PCD	Polycrystalline diamond
PVD	Physical Vapor Deposition
RA	Regression analysis
sc-cBN	Single crystal cubic boron nitride
SCD	Single crystal diamond
Ti	Titanium
TiAlN	Titanium aluminum nitride
TiC	Titanium carbide
TS	Tribological system
W	Tungsten
wBN	Wurtzitic Boron Nitride
WC	Tungsten Carbide

III List of figures

IV List of tables

1 Introduction

The global demand for superhard materials continues to rise, driven by intensive manufacturing activities. At the same time, demanding environmental legislation and materials recycling requirements call for new developments such as superhard materials for coolant-free or high-speed dry machining [ZHAO16, p. 2]. In particular, the application of these material in grinding processes plays a key role in the manufacture of cutting tools from extremely hard cutting materials such as PCD and pcBN. However, the high hardness H_V of these materials results in long processing times and high grinding wheel wear [VITS20, p. 38].

More into detail, cubic boron nitride (cBN) is the main focus of this work. This material is the second hardest material after diamond with great thermal stability and low fracture toughness K_{Ic}. In particular, it is possible to apply it at temperatures up to T = 2000°C [KANY16, p. 16]. Furthermore, it provides a lot of interest thanks to the insolubility in ferrous materials, cobalt, or nickel [XU15, p. 4]. Consequently, it is mainly used as an abrasive and as a substitute of diamond in particular occasions.

The application of diamond as a grinding material supposes a significant challenge due to the following reasons. On one hand, its transformation into graphite at high temperatures. On the other hand, the technical complexity that supposes the measurement of temperature T on a single grain of diamond. As a result of these reasons, tool-life prediction of diamond grinding wheels is highly influenced by temperature T. These facts make the study of heat distribution and maximum temperature in the workpiece T_{wp} on the contact zone A_W during grinding an interesting field of research to focus on.

Consequently, a further knowledge about these concepts offers the potential to increase the efficiency and profitability of the grinding of superhard materials. In particular, special interest is focus on pcBN. As a result of that, manufacturing costs will be reduced. For this purpose, further knowledge about the relationships between material properties and grinding parameters during pcBN grinding is required.

The incomplete knowledge about the relationships between grinding parameters and temperature T has a high influence on the grinding process design and tool-life depending on the pcBN specification. Therefore, this field of knowledge requires time-consuming and costly empirical tests in the manufacture of pcBN cutting materials. The resulting production costs increases the profitability of using pcBN as a cutting material.

Simulations about grinding process are conducted throughout this study. The objective of them is to provide an approach related to the problem stated previously. Consequently, temperature T predictions are achieved. This data enables the possibility of understanding the heat transfer mechanism through diamond and cBN single grains. For that purpose, software for programming, 3D designing, and Finite Element Analysis (FEA) will be applied.

Therefore, this thesis contributes to the study of the temperature T and heat distribution over the contact zone A_W of pcBN and PCD with the aim of further findings on the heat transfer mechanisms and thermal behavior of these materials.

2 State of the art

In the following, the basics, structure and synthesis of superhard materials are discussed first (section 2.1 and 2.2). Then, novel superhard materials with a special focus on polycrystalline cubic boron nitride and polycrystalline diamond is presented. Thereafter, a basic description of tribology and its application to grinding regarding the heat generated during processes is provided. In section 2.3, a description of surface grinding is presented including classification, tooling and cutting mechanisms. Finally, this chapter concludes with a brief description of methods for simulating grinding processes discussing advantages and drawbacks of every methodology commented.

2.1 Basics of superhard materials

Superhard materials are classified under the category of advanced materials. This kind are materials whose properties have been enhanced or newly developed high-performance materials. According to Klocke, most of these materials belong to the advanced ceramics under the category of non-oxidic ceramics (carbides, nitrides, borides, silicides...) [KLOC11, p. 171]. Specific properties belonging to this group of abrasive materials are explained in this section.

Firstly, one main property to focus on is hardness. Hardness is a mechanical property defined as the ability to resist deformation upon a load [VEPR99, p. 2402] or the ability of a material to resist being scratched or dented by another [XU15, p. 142]. In order to measure and compare it with other materials, there are numerous hardness tests such as the Rockwell, Vickers or Knoop tests [KAKA04, p. 246]. In particular, Knoop is more precise for superhard materials due to its smaller indentation angle. The Knoop indenter will last longer and does not force the hard material to crack as fast as with the Vickers indenter. This fact is based on the deep of penetration. The Knoop indenter penetrates only about half as deeply as the Vickers indenter for the same load [MARI15, p. 111].

When studying and comparing different materials with wide ranges of hardness values, the Vickers method is widely used as the standard because this technique offers the widest range of scales for hard materials [EN05, p. 6]. The hardness measurement unit is named Vickers Pyramid Number *HV*. This unit is expressed in MPa or GPa. According to Kanyanta materials can be classified into three categories. Hard materials with a hardness $H_V \leq 40$ GPa. Superhard materials with a hardness between 40 GPa < $H_V \leq 80$ GPa. Ultrahard materials with a hardness $H_V = 80$ GPa [KANY16, p. 4]. As a result of their high hardness, superhard materials are wear resistant. This characteristic is another interesting property which will be explained in more detail in section 2.2.

Thermal properties especially thermal behavior at high temperatures T are highly influencing in the working conditions considered in this study. A low thermal expansion α, high thermal conductivity λ and high thermal capacity C are the significant properties which define superhard materials [KAKA04, p. 400].

On the other hand, another property typical of superhard materials is brittleness or fracture toughness K_{Ic}. This property is defined as the material's property to fracture before deformation [KAKA04, p. 224] and is a big drawback since they are expected to work under conditions of high stress σ and force F.

Regarding the crystallography, atom distribution and lattice have a significant influence. In particular, most of these superhard materials have covalent bond [WENT80, p. 873]. This type of bonding provides greater interatomic strength because high quantity of energy is needed to remove these bonds. Sp^3 bond hybridization plays a big role due to the atomic distribution that develops. This structure is made of four orbitals developing a tetrahedral

structure. Thanks to this distribution, cubic boron nitride (cBN) and diamond achieve greater thermomechanical properties.

In order to provide a deeper description of superhard materials it is necessary to understand macroscopic properties. Mazhnik et al. stated that it is a great challenge to find the exact model, which tries to predict and correlate hardness H_V and other variables. These other parameters are macroscopic properties according to crystal structure, microstructure parameters, manufacturing and material processing [MAZH20, p. 128].

2.1.1 Classification and synthesis of superhard material

Several authors have tried to describe a proper classification of superhard materials. Some examples are the following. Vepřek divided superhard materials into intrinsic and extrinsic [VEPR99, p. 2401]. Wentorf et al. categorized materials under hardness groups. Common materials, harder materials and superhard materials. Into this last group only diamond and cBN was considered [WENT80, p. 874].

Nevertheless, currently there is no actual classification, where these materials are organized in specific groups. As mentioned previously, a possible classification would be under abrasive materials. Sometimes this group is mistaken by just considering ceramics. Nevertheless, it is possible to organize superhard materials by including most of the materials groups with hardness H_V in the range aforementioned. Therefore, these materials are polycrystalline cubic boron nitride (pcBN), single crystal cBN (sc-cBN), polycrystalline diamond (PCD), single-crystal diamond (SCD), nanostructured materials (NTM), nitrides and borides [SUMI16, p. 26].

Figure 2.1 shows ultrahard materials. These materials are generally NTM materials synthesized under very high pressure p and temperature T, as explained in section 2.2.3. As a result of that, as reported by Sumiya et al., only SCD and nanopolycrystalline diamond are included in this category [SUMI16, p. 24].

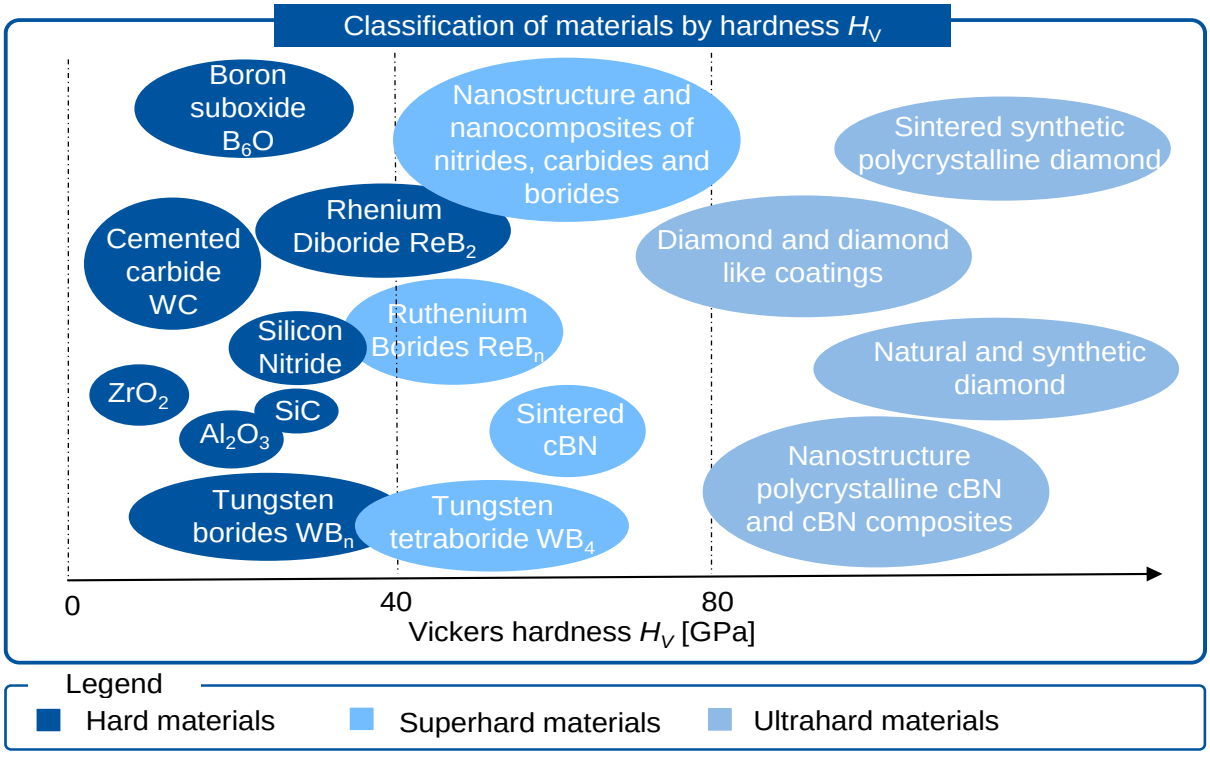

Figure 2.1: Classification of superhard materials by Vickers hardness H_V [KAY16, p. 4]

Currently more scientific interest and research is focused on NTM, nitrides and borides. This interest is based on the increase in demand for finding a cheaper solution. For that purpose, elements that does not need specific requirements are researched [KANY16, p. 17]. Some examples related to the components mentioned are light element compounds made of boron, carbon, nitrogen, and oxygen (BC_XN, BC_X, γB_{28}, B_6O) and compounds made of transition metals and light elements (B, C, and N) such as ReB_2, OsB_2, WB_4, FeB_4, PtC, IrN_2, OsN_2, and PtN_2 [XU15, p. 2].

Synthesis of superhard materials

Figure 2.2 shows high-value parameters of pressure *p* and temperature *T* for carbon and boron nitride. These values are needed in order to reach a phase transformation state where atoms are reorganized. To make that possible, processes like explosive/detonation techniques, laser ablation, high-energy ball milling at high pressure and high temperature (HPHT) and chemical vapor deposition (CVD) are used. In this section more attention is laid on HPHT and CVD because of their commercial application [MOCH12, p. 11].

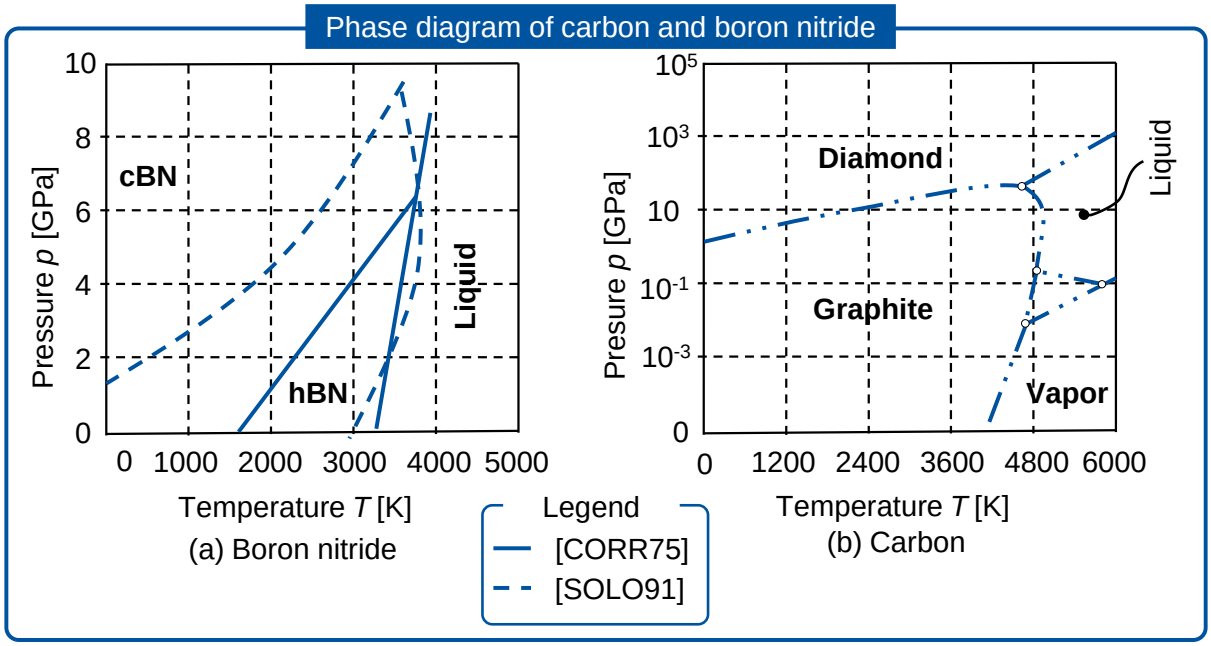

Figure 2.2: Phase diagram of carbon [BUND89, p. 172] and boron nitride [EYHU05, p. 13]

High pressure and high temperature synthesis

Figure 2.3.a shows the equipment specific for this method. This annealing technique is based on high temperature *T* and high pressure *p* depending on the material that is being produced [DOBR13, p. 23]. In addition, a catalyst is added to the base material with the aim of bonding with it. Generally, the technical equipment used for HPHT treatment are belt, toroid, BARS and cubic. The most common and basic one is BARS-300 with all its major parts. Moreover, special interest is laid on HPHT cells since the base material undergoes the phase transformation [DOBR13, p. 215].

Depending on the conditions of temperature T_{HPHT} and pressure p_{HPHT}, base, and binder material the final product will be obtained according to the properties and applications desired. Further information is provided in further sections according to each purpose.

Chemical vapor deposition

This process is defined as the deposit of material on a heated surface through a chemical reaction in the vapor phase [PIER99, p. 30]. Since a high temperature T_{HPHT} is needed to

synthetize superhard materials, two types of techniques are commonly used. These methodologies are thermal CVD or plasma CVD [ALCA16, p. 207].

In regard to manufacturing cBN, it can be produced by the plasma technique of electron-cyclotron-resonance (ECR) at T = 675°C. Also, it is accomplished with thermal CVD using diborane and ammonia diluted with hydrogen at T = 800°C. This technique is defined as hot filament chemical vapor deposit (HFCVD) [PIER99, p. 275]. In order to generate diamond with this procedure, the decomposition of a hydrocarbon (e.g., methane) is done by several methods but the most common ones are microwave plasma chemical vapor deposition (MPCVD) and HFCVD [ALCA16, p. 207]. As reported by Pierson, reaching a substrate temperature 800°C ≤ T ≤ 1000°C a deposition rate $\dot{r}$ 0.5 µm/h ≤ $\dot{r}$ ≤ 1 µm/h is achieved [PIER99, p. 207]. The equipment commonly used for HFCVD is shown in figure 2.3.b

Other procedures

Although diamond and cBN are the hardest materials in the world, thanks to the development of microscopic hardness models, there are two manufacturing strategies. One strategy is to design and synthesize novel superhard materials. The second strategy is to enhance hardness H_V of known materials through manipulation of their microstructure or coatings [ZHAO16, p.7].

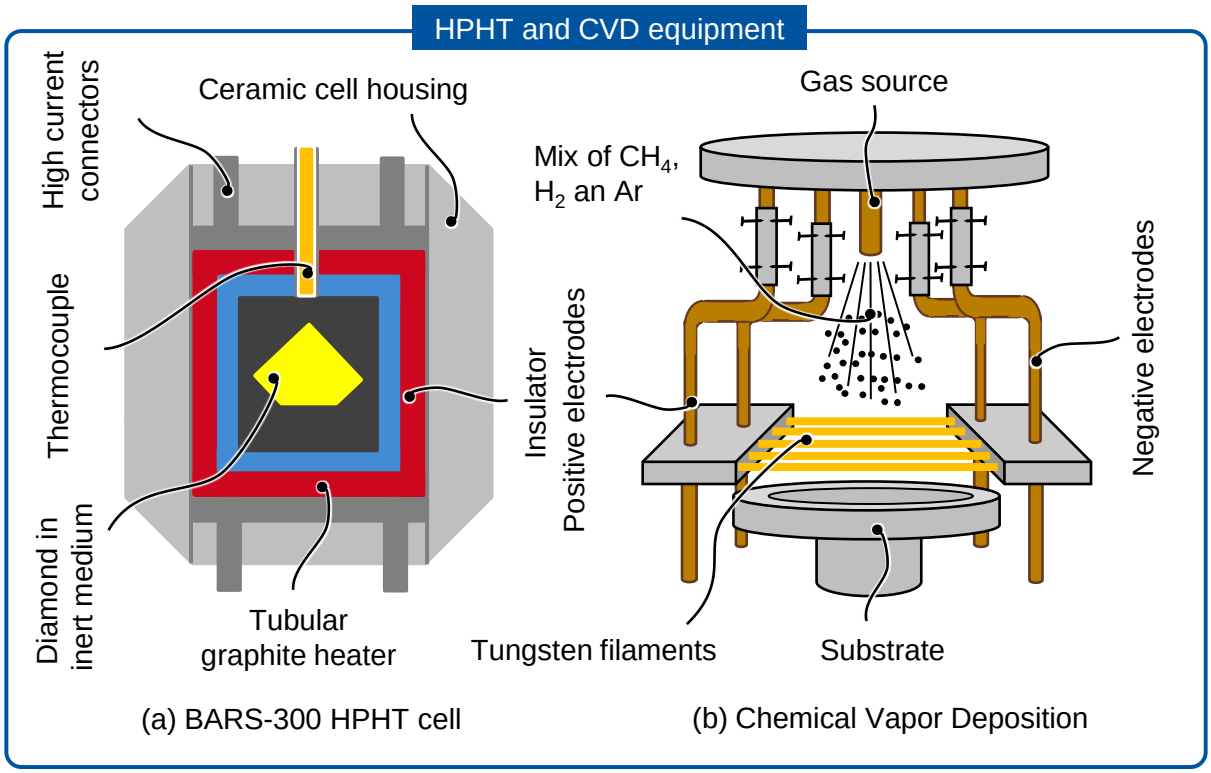

Figure 2.3: Equipment for HPHT [DOBR13, p. 215] and CVD processes [ALCA16, p. 209]

2.1.2 Microstructure of superhard materials

A brief idea about the microstructure and its behavior under plastic deformation is necessary to be introduced. To do so, the review of crystallographic concepts on beforehand are the following. First of all, every solid has an atomic organization defined as crystal lattice [KAKA04, p. 66] and the chemical bond that deploys this structure is ideally desired for superhard materials to be formed by ionic bonds. Nevertheless, it exists an exception of

diamond and silicon, which have covalent bonds and high hardness H_V, while other components with covalent bond have frequently lower hardness.

In addition, since hardness H_V is measured through plastic deformation of the surface, under a microstructure point of view, it is possible to define plastic deformation for single crystals as the movement of defects, either point defects or line defects depending on the temperature T, stress σ, and rate of deformation $\dot{\varepsilon}$ [KAPO17, p. 719]. Thus, some significant factors when studying hardness H_V are low dislocation mobility, high packing fraction or a high number of dislocations among others. Also, its correlation with superhard materials microstructure heavily influences plastic deformation of single crystals [JACK91, p. 35].

The movement of linear defects or, more precisely, dislocation mobility is also defined by the deformation mechanism known as slip deformation. This is the main mechanism for plastic deformation of microstructures. It is based on the movement of particles among slip planes in the crystal structure [KAKA04, p. 116]. The crystal structure takes a crucial responsibility as it depends on the distribution of atoms. Therefore, the possibility of having many slip directions increases. Consequently, the more slip directions, more slip planes to deform the crystal.

Figure 2.4 presents common lattice structures. These structures are the body centered cubic (BCC) and face centered cubic (FCC). These two crystal structures have more slip systems that allow better slip deformation at room temperature . However, hexagonal close-packed lattices (HCP) have limited slip systems which makes them more difficult to deform at room temperature. Nevertheless, the higher the temperature, the lower the difficulty to deform them. On the other hand, the polycrystalline structures dislocation movement is not that simple. In this case, the slip direction varies, due to their allotropy. This property is the nonuniform atom distribution throughout its structure. Hence, polycrystalline structures can support more plastic deformation compared to single crystals [KAKA04, p. 367]. Some examples of superhard materials are diamond and cBN with cubic structure which is very similar to FCC. This structure is presented in the subsequent section.

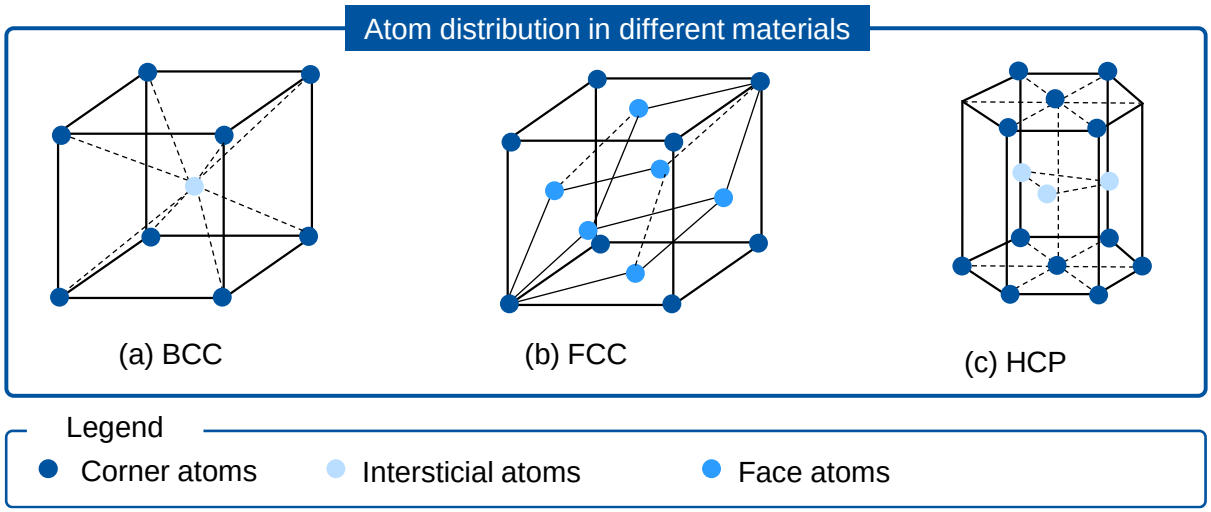

Figure 2.4: Atom distribution on different materials [KAKA04]

Structure of polycrystalline crystalline boron nitride

Boron nitride is a synthetic substance which was first synthesized by Wentorf in 1957. Also him patented its manufacturing process in 1961 [WENT61b]. This material has heavy similarities in atomic structure with diamond resulting in hardness H_V [WENT57, p. 956]. Boron nitride exists in different allotropic forms. Figure 2.5 presents the most commonly known the hexagonal , cubic and wurtzitic boron nitride [CORR75, p. 3812] . cBN is also known as zinc blended z-BN.

More attention is given to the cubic crystalline modification because of its abrasive characteristics and, therefore, the application in cutting processes. Compared to the other modifications and other materials, cBN has high hardness H_V . Its hardness H_V is not higher than diamond. Moreover, low fracture toughness K_{Ic} and good thermal stability. It is possible to apply it at temperatures up to T = 2000°C [KANY16, p. 16].This fact is due to its superconductor thermal conductivity $\lambda_{c\text{-}BN}$ = 1300 W/m·K [MORG98, p.667]. Moreover, it provides a lot of interest thanks to the insolubility in ferrous materials, cobalt, or nickel have led to a great deal of interest in introducing cBN as an abrasive [XU15, p. 4].

A polycrystalline structure is defined as a solid region composed of many grains randomly oriented and separated by grain boundaries [ANDE90, p. 88]. This structure is shown in figure 2.5. In order to obtain cBN in a polycrystalline solid structure there are two main possibilities. On one hand, direct conversion. On the other hand, conversion with catalyst. Direct conversion starts from hBN to cBN by a HPHT process which leads to binderless polycrystalline cubic boron nitride (bcBN) [BUND62]. In contrast, another possibility is a sintering technique where a binder component is added to the cBN crystalline grains, previously produced by techniques explained in the subsequent chapter. Aluminum, cobalt, nickel, or titanium are the most commonly used elements as binders to activate the sintering. These elements influence the application of the resulting material [GUOD14, p. 80]. Moreover, this sintering process is governed by three parameters. The starting material, pressurization and heating process conditions and conversion sintering temperature [SUMI16, p. 22]. This procedure previously explained is more common and traditional. Nowadays these conditions are not yet realistic for large-scale manufacture.

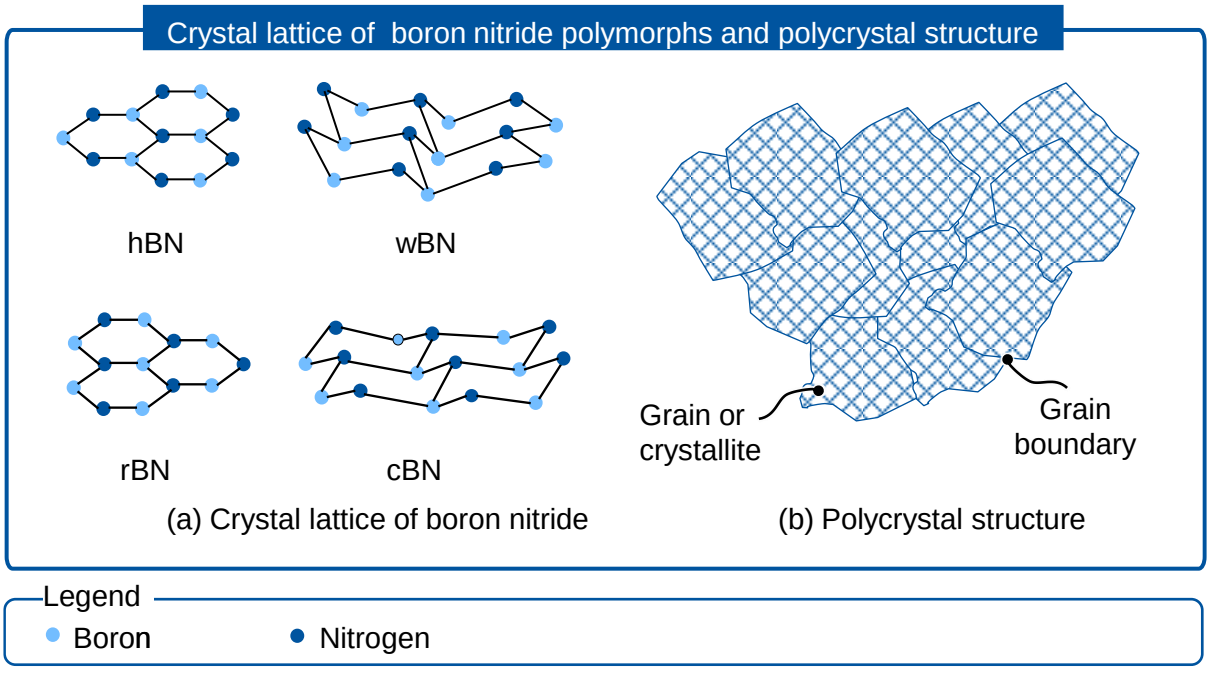

Figure 2.5: Crystal lattice of boron nitride polymorphs [PETR07] and polycrystal structure [ANDE90, p. 88]

Binder phase of polycrystalline cubic boron nitride

cBN is bonded with composite metals of the elements in groups IV-VI of the periodic table. These elements become the compounds of the binder phase. The choice of these elements is due to two reasons. On one hand, most of the interest laid on cBN applications is focused on cutting-tool industry (high-speed cutting). On the other hand, the bcBN manufacturing process is costly and limited in size [BENK99, p. 1838]. Therefore, common components found in binding phases are aluminum (Al), titanium (Ti), titanium nitride (TiN), titanium

aluminum nitride (TiAlN), titanium carbide (TiC), cobalt (Co), nickel (Ni) or tungsten (W) [KLOC11, p. 181].

As stated in ISO 513, cBN tools are classified under three groups depending on the cBN content. This groups are BL (low content of cBN), BH (high content of cBN) and BC (high content of cBN but coated) but the exact quantities are not specified [ISO12, p. 8]. According to Klocke, tools of the BL group are composed between 45% to 65% of pure cBN with a grain size smaller than 2 µm and a ceramic binder (e.g., TiC or TiN). Despite of the lower thermal conductivity λ of the binder compared to the grains, great characteristics of wear resistance, service life, and chemical stability are achieved [TANA16, p. 546].

More emphasis is laid on TiN binder because of its high influence in this work. This component is commonly used due to its high melting point, high hardness H_V, thermodynamic stability and resistance to chemical attack. According to Cho et al. when combined with boron nitride fracture toughness K_{Ic} is increased [CHO18, p. 658]. This component made of cBN, and TiN is usually applied in finishing operations of nickel-based alloys [KLOC11, p. 320].

BH materials are those where the cBN content $w_{c\text{-}BN}$ is above 80% with a grain size in a range of d_g = 0.5-10 µm in combination with a metallic binder (W-Co) or a ceramic phase based on Al or Ti [SLIP20, p. 429]. As is shown in figure 2.6, this kind of material has better thermal and mechanical properties compared to BL components. As reported by Tanaka et al., this kind of composition is the most recommended by the tool manufacturers regarding difficult-to-machine materials [TANA16, p. 545].

Finally, BC group is mainly focused on wear reduction and hardness H_V enhancement in order to increase tool-life service and productivity applying higher cutting speeds [SOO16, p. 89]. Usually, cBN tools are coated with TiN, TiAlN, aluminum chromium nitride (AlCrN) or aluminum oxide in a physical vapor deposition (PVD) process creating a layer of around 5 µm [SPRO96, p. 890].

Nevertheless, this binder phase is not a compulsory presence to obtain pcBN and thus by removing that part more purity is achieved. As a result of that, better thermomechanical properties without any residuals that becomes weak areas are obtained [FUJI09, p. 5649].

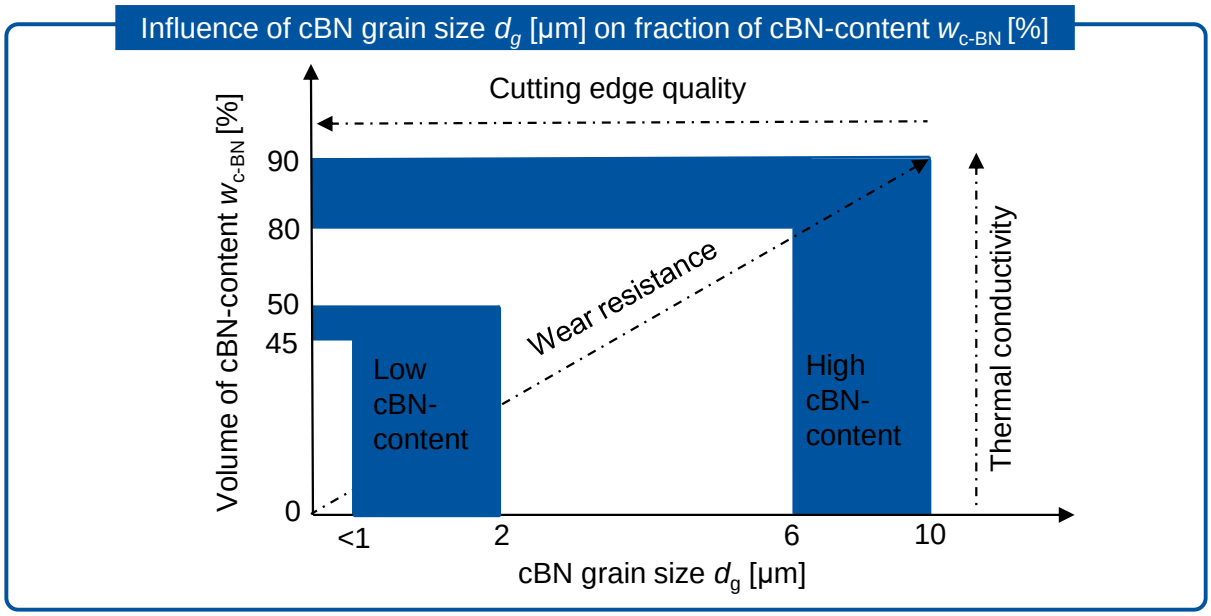

Figure 2.6: Influence of cBN grain size d_g [µm] with respect fraction of the cBN content $w_{c\text{-}BN}$ [%] [KLOC11]

Binderless polycrystalline cubic boron nitride

bcBN was firstly produced by Bundy et al. in 1963 [BUND63, p. 1144] and patented by Corrigan in 1967 [BUND67, p. 1]. One possibility of obtaining bcBN is by means of increasing the temperature 1300 °C ≤ T ≤ 2400 °C and pressure 8 GPa ≤ p ≤ 20 GPa. Wentorf et al. explained different procedures to obtain this product through different methodologies [WENT80, p. 208]. According to Sumiya et al., by reaching T_{HPHT} = 2200 °C and p_{HPHT} = 10 GPa a direct conversion is achieved. Hence, bcBN with d_g =100-300 µm grain sizes starting with h-BN as base material is achieved [SUMI14, p. 14].

Currently there is a trend of research around the study of these components thanks to the rise of hard-to-machine materials with special focus on titanium and cobalt superalloys. The main source of success of these materials is the lack of secondary phases which impede thermomechanical properties. Consequently, great wear resistance and high thermal conductivity λ are achieved [WANG05, p. 106]

Structure of polycrystalline diamond

Carbon exists in nature in different allotropic forms. One of them which can be diamond is found in nature and can also be synthesized. In 1955 diamond was synthesized for the first time [BUND55] and the process then patented in 1961 [WENT61a]. Figure 2.7 shows several forms, but the interest of this work is placed on two different configurations. In one hand, a hexagonal configuration known as graphite (figure 2.7.a). This form is the most stable under normal conditions of temperature T and pressure p. It is used as a lubricant due to its inter-planar Van der Waals bonds between hexagonal layers. On the other hand, the other interesting atomic configuration is cubic. This form is presented in figure 2.7.b and it is also known as diamond. In this case, it is bonded via covalent bonds [LOOS15, p. 74].

Interest is focused on the cubic form due to its thermomechanical properties. First of all, extremely high hardness H_V (70 GPa < H_V ≤ 100 GPa), and thermal conductivity λ define this material. It has two main downsides. On one hand, its low fracture toughness K_{Ic} due to brittleness. On the other hand, low thermal stability due to its behavior previously explained [JIAN20, p. 21527].

As stated by Sumiya et al., impurities from Ni and Bo play an important role during the manufacturing process. The thermomechanical properties will be modified depending on their concentration among its structure [SUMI96, p. 1360]. Although the attention given to diamond in this study is centered on abrasive applications, it is also widely used in the oil and gas drilling industry [CHEN20, p. 1]. Furthermore, PCD is mainly applied for non-ferrous materials such as high-silicon aluminum alloys, metal matrix composites (MMC) or carbon fiber reinforced plastics (CFRP) [ARSE05, p. 486].

Similarly to pcBN earlier mentioned, diamond is manufactured via two processes. On one side, PCD is manufactured by Chemical Vapor Deposition (CVD). On the other side, HPHT procedure generates different types of diamond according to the absence or presence of catalysts. These components define a binder phase. Consequently, thermomechanical properties will be modified. As a result of that, as reported in ISO 513, diamond is classified in three groups. This classification is divided in DM (monocrystalline diamond), DD (polycrystalline diamond without binder), and DP (polycrystalline diamond with binder) but exact quantities are not specified [ISO12, p. 8].

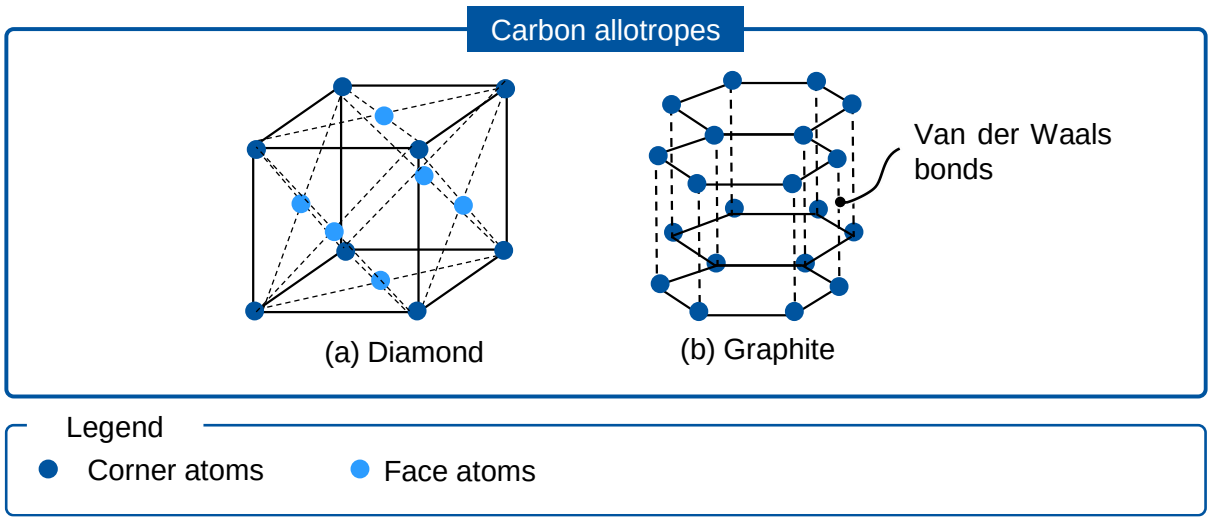

Figure 2.7: Allotropic structures of Carbon. Cubic (a) and hexagonal (b) [KANY16]

Binder phase in polycrystalline diamond

DP is found bonded with metallic binders. These components are usually cobalt, silicon, tungsten or tungsten carbide sintered with diamond grains with a size within d_g = 2-25 µm under conditions of high pressure 6 GPa ≤ p_{HPHT} ≤ 7 GPa and temperature 1400 °C ≤ T_{HPHT} ≤ 2000 °C [KLOC11, p. 175]. According to Li et al., cobalt is the most common binder in PCD tools formed together in a substrate of tungsten carbide [LI20, p. 402]. Cobalt is mainly used as binder for heat resistance, wear, and strength enhancement in PCD. Moreover, the great bonding with carbon particles is another reason for its application [CHEN20, p. 1]. Although SiC is also used as binder, it limits thermal stability [KLOC11, p. 178]. Lastly, WC is used as substrate for reducing manufacturing cost and for increasing insert size.

Binderless polycrystalline diamond

DD is obtained by direct conversion of graphite under conditions of high pressure and high temperature. Also, CVD processes are possible but take longer. As stated by Irifune et al., DD is achieved by sintering pure graphite (99,9995%) at pressure 12 GPa ≤ p_{HPHT} ≤ 25 GPa and temperature 2300 °C ≤ T_{HPHT} ≤ 2500 °C with a grain size d_g 10 nm ≤ d_g ≤ 20 nm [IRIF03, p. 599]. Furthermore, Sumiya et al. showed that these nano-diamonds have the highest hardness H_V and better thermal stability than other superhard materials such as pcBN, bcBN or DP [SUMI16, p. 23]. Finally, as stated by Mochalin et al., most of the applications focus on biomedicine or magnetic sensing [MOCH12, p. 17]. Industrial application is still under development since large-scale manufacturing is not possible yet. Also, these products are limited in size.

2.1.3 Intermediate conclusion

Superhard materials are advanced ceramics with great thermal and mechanical properties. On one hand, mechanical properties such as hardness H_V, abrasiveness and wear resistant are noticeable characteristics in most of the members of this group. On the other hand, thermal properties like thermal expansion α or thermal conductivity λ represent these materials as well. According to its hardness H_V, pcBN, sc-cBN, PCD, SCD, NTM, nitrides and borides are classified as superhard materials [SUMI16, p. 26]. Although general materials have BCC, FCC and HCP atom structure, most of the superhard materials have amorphous atom structure that prevents their movement.

In regard to its manufacturing process, two main methodologies are commercially available HPHT and CVD. HPHT relies on the conditions of high temperature T_{HPHT} and pressure

p_{HPHT}, base, and binder material. Depending on these characteristics, the final product will be obtained according to the properties and applications desired. In contrast, CVD is the deposition of material on a heated surface through a chemical reaction in the vapor phase at high temperature T_{CVD}. As previously mentioned, depending on this production conditions, different characteristics will be obtained.

cBN and diamond were commented throughout this section. On one side, cBN has a high hardness H_V, good thermal stability, low fracture toughness K_{Ic} and insolubility in ferrous materials, cobalt, or nickel. This last property is the main advantage against diamond. Also, it can be found in different forms depending on the fraction of cBN on its content w_{cBN} and with the presence or absence of binder. This binder is made of several materials such as TiN, TiAlN or TiC. On the other side, diamond extremely high hardness H_V and thermal conductivity λ, low fracture toughness K_{Ic} and low thermal stability. Similarly to cBN, this material can be found in 3 groups according to its binder phase DM, DD and DP.

2.2 Tribology applied to face-surface grinding processes

2.2.1 Introduction to tribology

Tribology comes from the Greek root τριβω (tribo) which means to rub and the suffix λόγια (logia) which means science [LUDE19, p. 1]. As stated in DIN 50323, it is defined as the science and technology of surfaces acting on each other in relative motion [DIN88, p. 1]. As a result of that contact, huge energy losses occur. In order to reduce them, several disciplines study this field of knowledge such as solid mechanics, fluid dynamics, material science or chemistry [LUDE19, p. 4].

More detail is given in this study for interactions between elements surfaces in grinding processes. For that purpose, the abstraction into a complex tribological system (machine, grinding fluid, atmosphere…) is done. Then, this fact enables the understanding of the agents and the mechanisms necessary to describe properly these series of phenomena. Furthermore, in this work specific interest is laid on heat generation due to friction [ROWE14, p. 23].

Tribological system

Tribological system (TS) is the conjunction of elements with absence or presence of wear, friction, chemically enhanced loss of material, mechanical loads of two surfaces and lubrication [LUDE19, p. 212]. As reported in DIN 50320, a TS is characterized by the materials involved in the wear process and their tribological properties and interactions between them. These elements are the following (figure 2.8). Base body (1), element that suffers the motion done by the counter body. Counter body (2), element which executes a relative movement against the base body. Intermediate medium (3), separation between effective contact zones. Surrounding medium (4), external environment that surrounds and encloses the system [DIN79, p. 4]. Depending on the surrounding mediums characteristics, tribological systems are classified under two groups closed TS and open TS. On one hand, closed TS are ideally isolated from the natural environment. Consequently, this prevents the exchange of substances and energy with the outside world (e.g., gearbox or valves in an internal combustion engine). In contrast, open TS are affected by the surrounding medium (e.g., weather conditions such as temperature, humidity, pressure…) [LYU16, p. 1]. Furthermore, according to Holler, stress components that affect the TS are mainly influenced by normal force F_n, temperature T, speed v, and duration of the stress t_{stress} [BREV04].

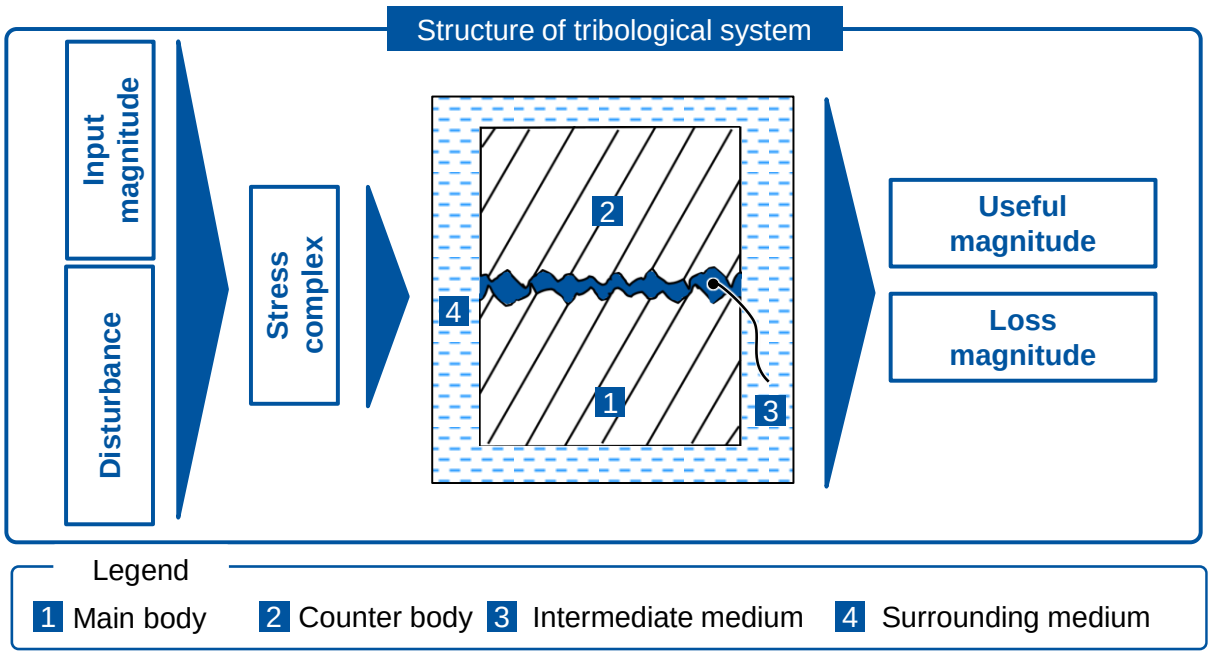

Figure 2.8: Tribological system and its structure [BREV08]

Mechanisms of tribology

Tribology is based on three pillars thanks to which it explains all the physicochemical interactions among surfaces. These three concepts are the following. Wear, lubrication, and friction. In order to have a further understand on tribology, a brief description of these three concepts is subsequently explained.

Wear

As reported in DIN 50320, the mechanism of wear is defined as the progressive loss of material from the surface of a solid body brought about by mechanical causes, i.e. the contact of a solid, liquid, or gaseous counter body [DIN79, p. 1]. Another definition was reported by Ludema et al., as the succession of events whereby atoms, products of chemical conversion, fragments, et al., are induced to leave the tribological system [LUDE19, p. 153]. As mentioned earlier, material properties such as hardness H_V or fracture toughness K_{Ic} or coatings are highly correlated with this mechanism. Noticeable attention is laid on it by the cutting-tools industry due to its relation to wear as well as to its service life. Wear occurs mainly because of four mechanisms presented in figure 2.9. These mechanisms are abrasion, adhesion, corrosion, and surface fatigue [KRAU74, p. 123].

Figure 2.9.d shows abrasion. This mechanism is the result of the displacement of material from one of the two sliding surfaces of the counter body caused by the relative hard asperities and the interaction with the particles in the intermediate medium [KRAU74, p. 125]. Secondly, adhesion is shown in figure 2.9.a. Adhesion is defined as the formation of bonds between certain molecules, according to Kraus, mostly in metallic surfaces. Due to the relative movement between the main body and counter body, these bonds are deformed, reinforced, and sheared-off. Consequently three defacements are caused. These defacements are micro-plowing, micro-cutting, and microcracks [KRAU74, p. 123]. Thirdly, corrosion showed in figure 2.9.c, also defined by Klocke as “tribooxidation”. This mechanism is the acceleration of chemical or electrochemical reactions due to the relative motion among all components in the TS. In most cases this process is slow and is prevented by additives found in lubricants [KRAU74, p. 126]. Finally, figure 2.9.b shows surface fatigue. It is the fatigue cracking due to alternating and cyclic stresses which results in the breaking away of a surface part. These series of operations have a long incubation period where no measurable wear occurs [KRAU74, p. 126].

Lubrication

The introduction of any material in between two sliding surfaces is defined as lubrication [KRAU74, p. 127]. The intermediate medium in the TS is responsible for this purpose which aims for reducing the effect of the other two aforementioned tribology mechanisms [KLOC11, p. 220].

Moreover, lubrication is classified under three different situations. These groups are liquid film lubrication, boundary film lubrication and films of solid lubrication [LUDE19, p. 112]. In addition, Kraus also includes no lubrication or dry friction under this classification [KRAU74, p. 128].

First of all, liquid film or full fluid lubrication consists of an ideal condition where the forces are completely transmitted through the lubricant film. Moreover, there is no contact between main body and counter body ($0.001 \leq \mu \leq 0.01$). Secondly, as reported by Kraus, boundary lubrication is the presence of lubricant with more than 99% of the surfaces in contact [KRAU74, p. 128]. In contrast, Ludema et al., defined it as the growth of an oxide or other soft surface reaction product due to the additives in the aiming to reducing friction. Films of solid lubrication are a type of lubrication where a solid material with lower shear strength appears compared to the main contact zones being lubricated (e.g., silver (Ag), lead (Pb) or graphite) [LUDE19, p. 112]. Finally, no lubrication or dry friction is the absence of lubricant, so it is a pure contact between surfaces ($\mu \geq 1$) [KRAU74, p. 128].

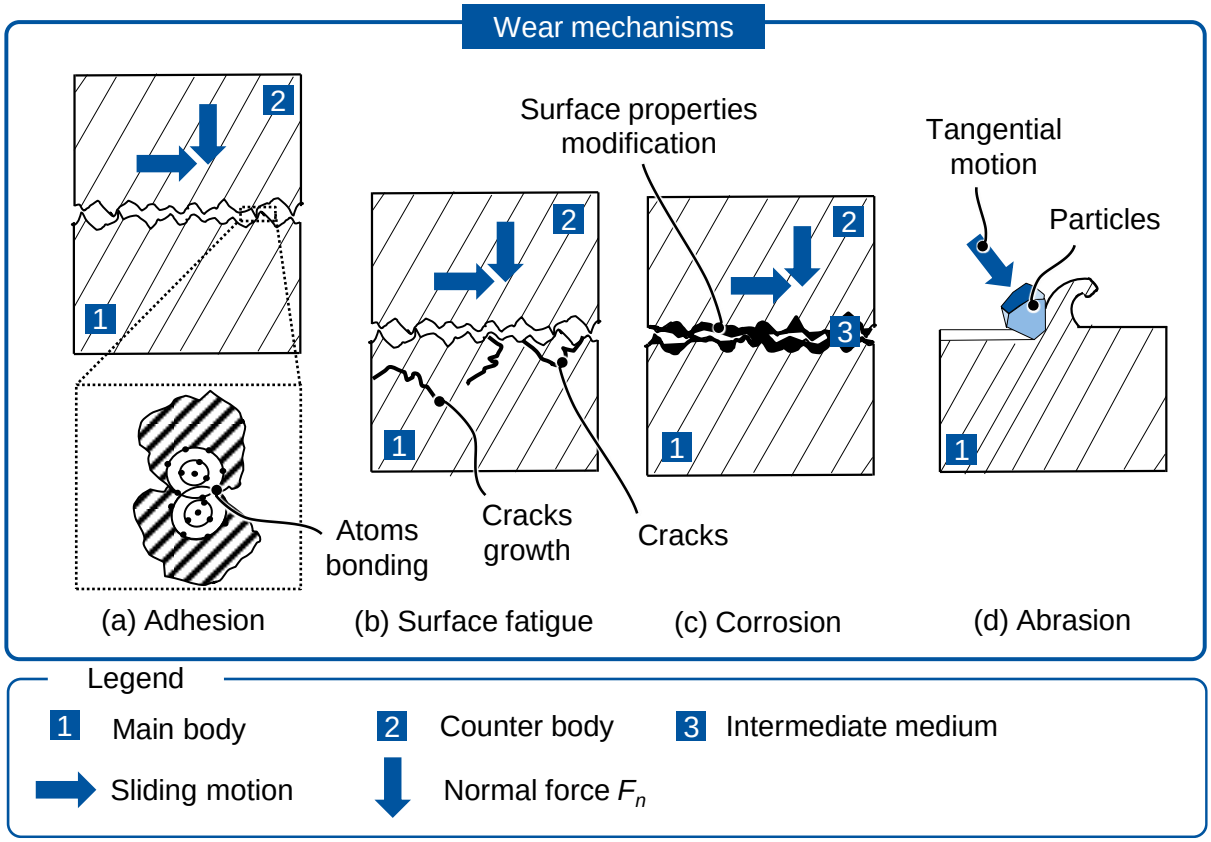

Figure 2.9: Types of wear mechanisms [KLOC11, p. 74]

Friction

As stated by Kraus, the resistant force that needs to be overcome on two surfaces pressed together in order to slide one over the other is defined as friction [KRAU74, p. 122]. It is

described in terms of a coefficient and is usually erroneously assuming it as constant and specific to each material [LUDE19, p. 73].

Adhesion is highly related to friction and wear. According to Ludema et al., every pair of contacting substance is under adhesion, although it is not profoundly understood. Therefore, all mechanisms of friction and wear should be referred to as adhesive mechanism [LUDE19, p. 82]. On the other hand, Kraus explained friction using several theories where one of them is adhesion [KRAU74, p. 122]. Friction is the cause of the forces that occur during grinding, and the root cause of the heat generation on the contact zone A_w which will be reviewed in the next section.

2.2.2 Forces resulted of friction

As reported by Klocke, equation 2.1 shows the main grinding force which is divided in three components. The decomposition is normal, tangential, and axial. Figure 2.10 presents this decomposition [KLOC09, p. 171].

The normal force F_n acts radially upon the grinding wheel and is responsible for the machine and workpiece deformation. The tangential force F_t engages in the peripheral direction of the grinding wheel. Both forces previously mentioned are a result of the angular spinning of the grinding wheel in contact with the workpiece. They are used to characterize the friction in the contact zone. Finally, the axial force F_a acts in the parallel direction to the grinding wheel rotational axis [KLOC09, p. 171].

$$\vec{F}_c = \vec{F}_t + \vec{F}_n + \vec{F}_a \tag{2.1}$$

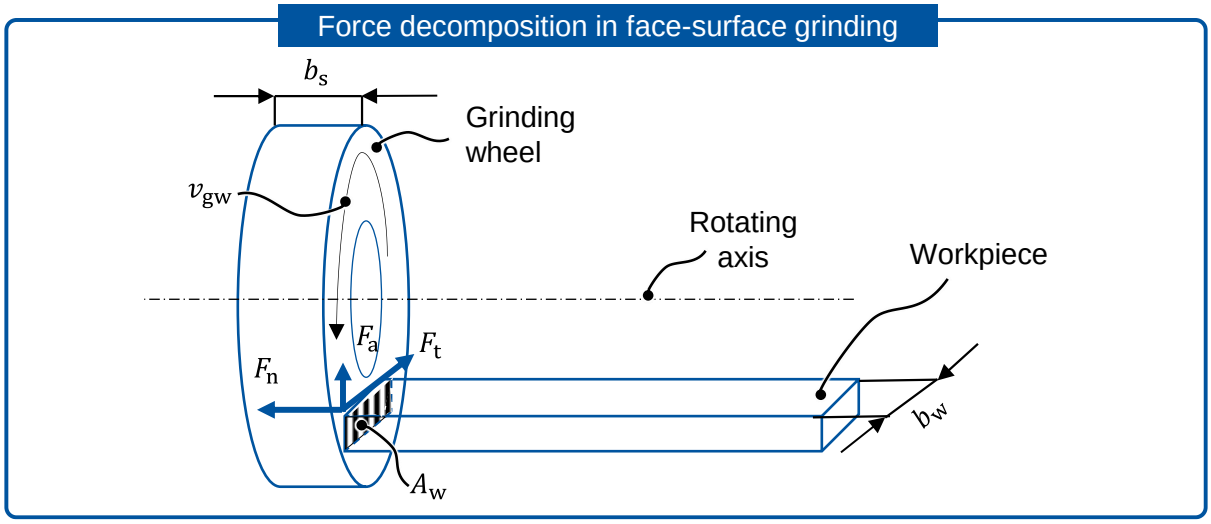

Figure 2.10: Force decomposition in the contact area A_w in face-surface grinding [DIN03]

Analytically these components are determined as:

$$F'_n = \frac{F_n}{b_{s,eff}} = \int_0^{l_g} k \cdot A_{cu}(l) \cdot N_{kin}(l) \cdot dl \tag{2.2}$$

As stated in equation 2.2 the specific normal force F'_n, which is the normal force F_n on the width of the active grinding wheel profile $b_{s,eff}$ is described.

$$F_a = E_w \cdot A_w \cdot \frac{\Delta l_w}{l_w} = E_w \cdot A_w \cdot \frac{l_{w_f} - l_{w_o}}{l_w} \tag{2.3}$$

Equation 2.3 shows the estimation for axial force F_a (normal force F_n as reported by Popov) in a contact between an elastic parallelepiped (workpiece) and a rigid plane due to compression forces. In our study this plane is the one of the grinding wheel [POPO10, p. 74].

$$G = \frac{F_t}{v_{rel}} \approx 2 \cdot G^* \cdot a_e \quad \textbf{(2.4)}$$

*: Efective shear modulus

$$G^* = \frac{G_2 \cdot (2 - \nu_1) + G_1 \cdot (2 - \nu_2)}{4 \cdot G_1 \cdot G_2} \quad \textbf{(2.5)}$$

$$v_{rel} \approx \frac{\pi \cdot \tau_o \cdot a_e}{G^*} \quad \textbf{(2.6)}$$

$$F_t \approx 2 \cdot G \cdot a \cdot v_c \approx 2 \cdot \pi \cdot \tau_o \cdot a_e^2 \quad \textbf{(2.7)}$$

Equation 2.4 shows the approximation for the tangential force F_t in a contact between a half-space and a rigid body, which is a good approximation for the understanding of this mechanical process [POPO10, p. 122]. This equation is composed by the effective shear modulus G^*, defined in equation 2.5, and the depth of the cut a_e. Consequently, equation 2.7 defines the tangential force F_t by substituting the cutting speed v_c into equation 2.4. As a result of that, the initial stress τ_o component appears in the final equation.

In order to introduce the heat generated, it is imperative to explain that the largest amount of mechanical energy introduced to the process is converted to heat during grinding. Therefore, according to Klocke, specific grinding power P'_c, defined in equation 2.8, is equal to the total heat flow q_t introduced during the grinding process [KLOC09, p. 172].

$$P'_c = \frac{F'_t \cdot v_c}{l_g} = \frac{F'_t \cdot v_c}{\sqrt{d_s \cdot a_e}} \quad \textbf{(2.8)}$$

$$P'_c = q_t \quad \textbf{(2.9)}$$

Equation 2.8 shows the specific cutting power P'_C transferred. This equation is a function of the specific tangential force F'_t, cutting speed v_c and the geometrical contact length l_g which is defined by grinding wheel diameter d_s and depth of cut a_e.

Heat generation

As reported by several authors, most of the power transferred to the workpiece is converted into heat. This heat is transmitted through the contact zone A_W between grinding wheel and workpiece. The heat provided during grinding processes is conducted away by workpiece, chips, grinding wheel and cooling lubricant. Depending on the grinding method applied, heat is transferred in different manners. Since the grinding technique which is going to be applied is surface grinding the following equations are related to this process [KLOC09, p. 173].

From an analytical point of view, as previously said, total heat flow q_t is divided into four parts as shown in equation 2.10. Heat flow in chips q_{sp}, heat flow in cooling lubricant q_{kss}, heat flow in workpiece q_w and heat flow in grinding wheel q_s [KLOC09, p. 173]. In agreement with several authors, this heat flow partitioning is determined with the goal of reaching a precise prediction of the temperature in the grinding zone [MALK07, p. 760].

$$q_t = q_{sp} + q_{kss} + q_w + q_s \quad \textbf{(2.10)}$$

In addition, Klocke explains that each component of equation 2.10 is defined as a part of the total heat flow q_t by a factor corresponding to specific characteristics depending on the process.

$$R_{sp} + R_{kss} + R_w + R_s = 1 \quad \textbf{(2.11)}$$

As reported by Klocke, each component is defined as [KLOC09, p. 173]

$$q_{sp} = R_{sp} \cdot q_t = \frac{\rho_w \cdot c_w \cdot T_{sp}}{e_c} \cdot \frac{F_t' \cdot v_c}{\sqrt{d_s \cdot a_e}} \quad \textbf{(2.12)}$$

$$e_C = \frac{F_t \cdot v_c}{Q_w} \quad \textbf{(2.13)}$$

$$Q_w = a_e \cdot v_w = a_e \cdot \pi \cdot d_w \cdot n_w \quad \textbf{(2.14)}$$

First of all, the heat transferred through the chips q_{sp} is described by equation 2.12. This equation is a function of numerous components such as the specific griding energy e_c which is required for the material removal of a volume element.

$$q_{kss} = R_{kss} \cdot q_t = \frac{(T_{kss} - T_o) \cdot h_{kss} \cdot l_g}{e_c \cdot Q_w'} \cdot \frac{F_t' \cdot v_c}{\sqrt{d_s \cdot a_e}} = \frac{(T_{kss} - T_o) \cdot h_{kss} \cdot F_t' \cdot v_c}{e_c \cdot Q_w'} \quad \textbf{(2.15)}$$

$$Q_w' = \frac{Q_w}{b_{s,eff}} \quad \textbf{(2.16)}$$

By means of equation 2.15 heat transferred via the coolant q_w is described

$$q_w = R_w \cdot q_t = \sqrt{k_w \cdot \rho_w \cdot c_w} \cdot \sqrt{r_o \cdot v_s} \cdot \frac{F_t' \cdot v_c}{\sqrt{d_s \cdot a_e}} \quad \textbf{(2.17)}$$

In contrast, equation 2.17 describes the heat flow through the workpiece q_w.

$$q_s = R_s \cdot q_t = 0{,}97 \cdot k_g \cdot \frac{F_t' \cdot v_c}{\sqrt{d_s \cdot a_e}} \quad \textbf{(2.18)}$$

Finally, in equation 2.18 the heat flow via the grinding wheel q_s is shown.

Thermal distribution models for calculating surface temperatures during grinding

In this section models for heat distribution during grinding are described. These heat distribution models are the single grain model [GUO99, p. 248], composite model [MALK07, p. 772] and heat distributions for unusual situations [MARI12, p. 149].

Figure 2.11.a shows the single grain model. This model includes the heat transferred to the abrasive grains, fluid, and workpiece by considering a grain surrounded by fluid. Moreover, it can be applied in different grinding and fluid applications such as regular or creep-feeding grinding [MALK07, p. 772]. In contrast, composite model describes how the grinding wheel and fluid are considered as a composite, i.e. one unique component. As a result of that, the manner to estimate energy partition becomes relatively simple by equating the maximum temperature rise at the grinding zone and maximum temperature rise on the composite. Then, a triangular heat source in the workpiece is achieved [GUO00, p. 153].

Finally, as stated by Marinescu et al., the heat transferred into the workpiece is a cumulative average of very short bursts of intensive energy defined as heat pulse. These pulses are result of the contact between workpiece and grain. Moreover, a section of the workpiece will experience many pulses over a long duration t_{pulse} = 10.000 µs with a contact duration of

$t_{contact}$ = 100 µs per grain. Every possible heat pulse is shown in figure 2.11.b [MARI12, p. 149].

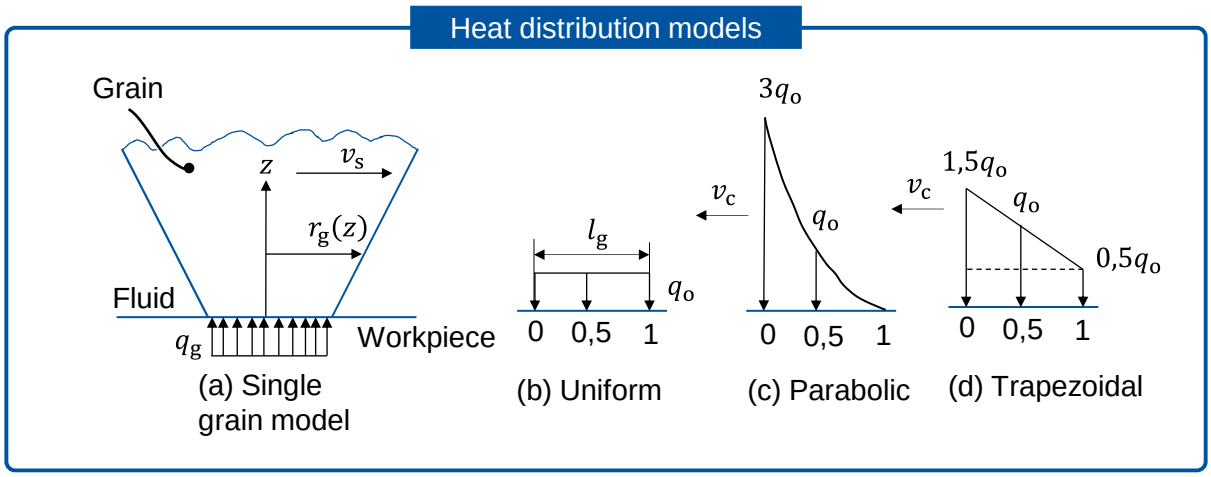

Figure 2.11: Different models of heat distribution [MARI12] [MALK07]

2.2.3 Intermediate conclusion

Tribology is a multidisciplinary science that acquires numerous fields of knowledge. A TS is used to explain the components which interacts in a system. For that purpose, this TS is divided in four parts. These parts are base body, counter body, intermediate medium and surrounding medium. Depending on this last one, TS can be classified into closed systems or opened systems. Moreover, this science is supported by four mechanisms. These mechanisms are wear, lubrication and friction. First of all, wear is the progressive loss of material from the surface of a solid body brought about by mechanical causes which are abrasion, adhesion, corrosion, and surface fatigue. Then, lubrication is the introduction of any material in between two sliding surfaces. In the TS corresponds to the intermediate medium. It is classified under three categories. These three categories are liquid film lubrication, boundary film lubrication and films of solid lubrication. Finally, friction is the resistant force that needs to be overcome on two surfaces pressed together in order to slide one over the other. As a result of this, cutting force F_c occurred which is divided in normal, tangential, and axial. Normal force F_n acts radially upon the grinding wheel and is responsible for the machine and workpiece deformation. Tangential force F_t engages in the peripheral direction of the grinding wheel. Axial force F_a acts in the parallel direction to the grinding wheel rotational axis.

Due to the composition of tangential force F_t and grinding wheel speed v_s, grinding power P_c is generated. Consequently, mechanical and heat loads are occurred in the workpiece while grinding. The heat load is transferred into four components. These components are chips q_{sp}, cooling lubricant q_{kss}, workpiece q_w and grinding wheel q_s. Moreover, several models for describing the heat distribution are single grain model, composite model and heat distributions for unusual situations

2.3 Grinding of superhard materials

2.3.1 Classification of grinding

As reported in DIN 8580, manufacturing processes are classified into six groups where grinding belongs to “cutting” group (3), which is also divided in 6 groups. One of these groups is machining with geometrically undefined cutting edges (3.3) where it is possible to find other processes such as honing, jet cutting or lapping. Moreover, this standard also

divides the previous group in 7 different ones, where one of them is grinding with rotatory tools (3.3.1) [DIN20, p. 8].

In addition to the aforementioned standard, DIN 8589-11 divides grinding with rotatory tool processes in six more categories. Under this division, the process which will be studied belongs to the group “surface grinding” (3.3.1.1). Finally, under this category the process “longitudinal side - face grinding” (3.3.1.1.3.1.) is the one chosen for this study since the morphology of the experiment simulated is similar to the one earlier commented. [DIN03, p. 14].

Characteristics of face-surface grinding

This manufacturing process is a cutting technique with different cutting edges (grains), as it is shown in figure 2.13, which generally is required for obtaining highly accurate tolerances. As reported by Klocke, the main purpose of this process is to create completely leveled surfaces or extend in the main feed direction of the grinding wheel in a straight line. For the application of this method, can be identified creep feed grinding and pendulum grinding. On one hand, creep feed grinding is based on large depths of cut in one overrun of the solid. In most of the cases it is applied for finishing operations. On the other hand, pendulum grinding aims for higher number of grinding paths and lower depth of cut. Therefore, better workpiece roughness and, higher grinding wheel wear are achieved [KLOC09, p. 233].

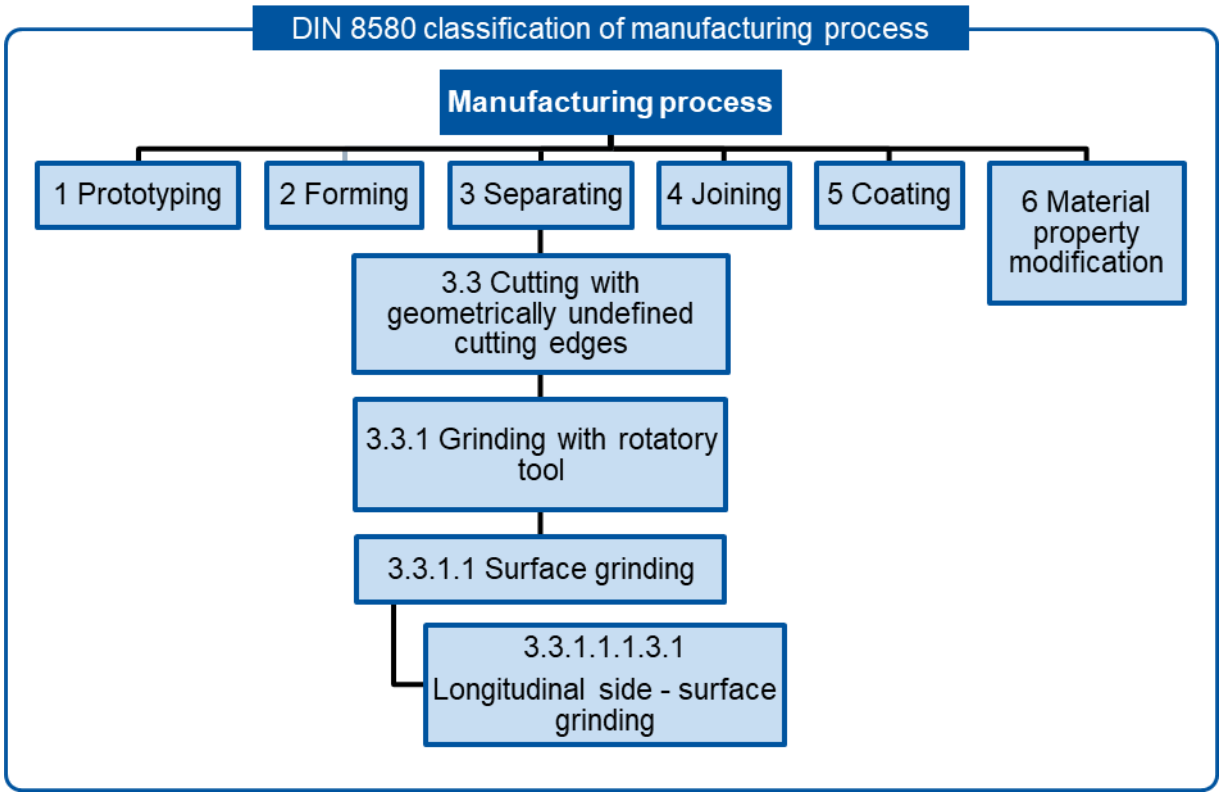

Figure 2.12: Classification according to DIN of manufacturing processes [DIN03]

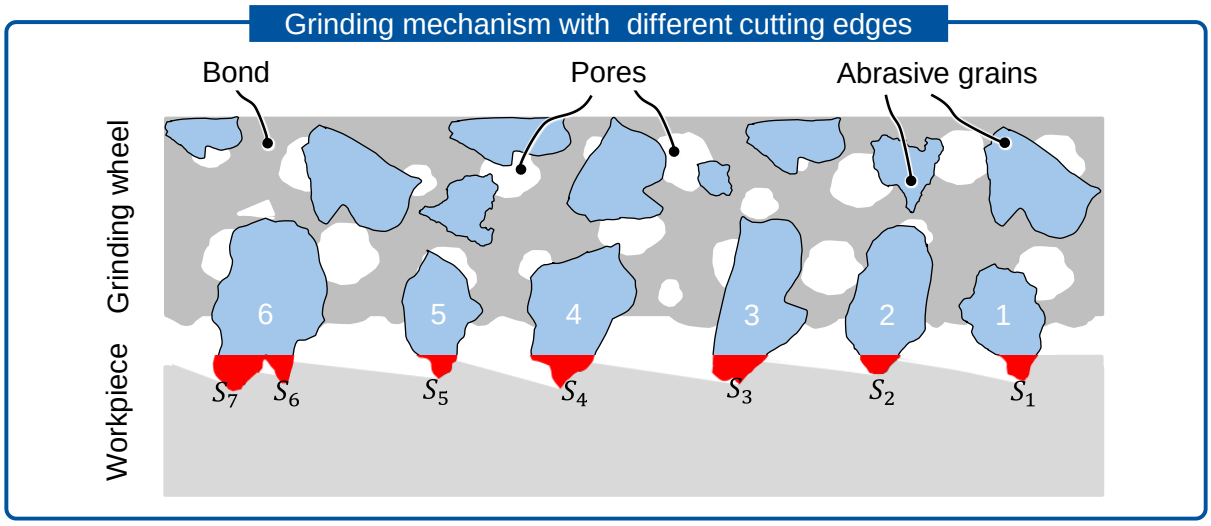

Figure 2.13: Cutting edges in the grinding wheel [KLOC09]

2.3.2 Superabrasive grinding tool

The grinding wheel is the instrument which is responsible for removing material. The main objective of this material removal operation is to achieve the required tolerance. In this subsection the principal components are presented.

Structure of grinding tool

Figure 2.14 shows the grinding wheel composition. It is composed by base body and abrasive coating. On one hand, the base body is the main frame where the abrasive coating is placed. Generally, this part is made of ceramic or metallic materials. In contrast, the abrasive coating is the composite made from the bond and grit materials. The bond is responsible for adhering to the grit and it is possible to differentiate distinct types which are explained in subsequent sections. Finally, grit materials can be found as single or multi-layer grains of the components with superabrasive characteristics as previously mentioned [KLOC09, p. 60-73].

Grit materials

Under this category several materials can be found. As reported by Klocke, these materials are natural or synthetic. Firstly, natural grit materials applied for industrial purposes are quartz, emery, garnet, and diamond. Except for natural diamond, the rest of materials mentioned do not have good mechanical characteristics when comparing to synthetic grit materials [KLOCK09, p. 17]. Synthetic grit materials are mainly corundum, silicon carbide, cBN, and synthetic diamond which, as explained in section 2.1 a wide variety of thermomechanical properties belong to this group [KLOCK09, p. 19]. Classification of and information about these materials are presented in DIN 69111.

Bond types

Grinding wheels bonds are divided in resin, vitrified and metal. Primarily, resin bonds are synthetic resins or a combination of synthetic resins with fillers without air in its structure. For that purpose, the most commonly used materials are phenol resins and phenol plasters. These last commented ones provide high resistance to shock and impact. Grinding wheels with this kind of resin are used for polishing or smoothing operations [KLOC09, p. 38]. Secondly, vitrified or ceramic bonds are composed by mixtures of white clay, kaolin, feldspar or quartz with frits as an additive, but there are commonly boron silicates or glasses containing magnesium with pores among their composition found on the market. Moreover,

depending on the quantity of glass phase added, different properties will be achieved. Their common properties are low fracture toughness K_{Ic}, high young modulus E, thermal stability and chemically resistant to oil and water [KLOC09, p. 39]. Finally, metallic bonds are found in different varieties, but mostly copper/TiN and cobalt bronzes are used, although it is also possible to find carbide bonds (W or WC). One main characteristic of these bonds is the strong and tight union established. Also, higher thermal conductivity λ compared to other bonds is obtained. Consequently, their main properties are high thermal conductivity λ and resistance to wear [KLOC09, p. 82].

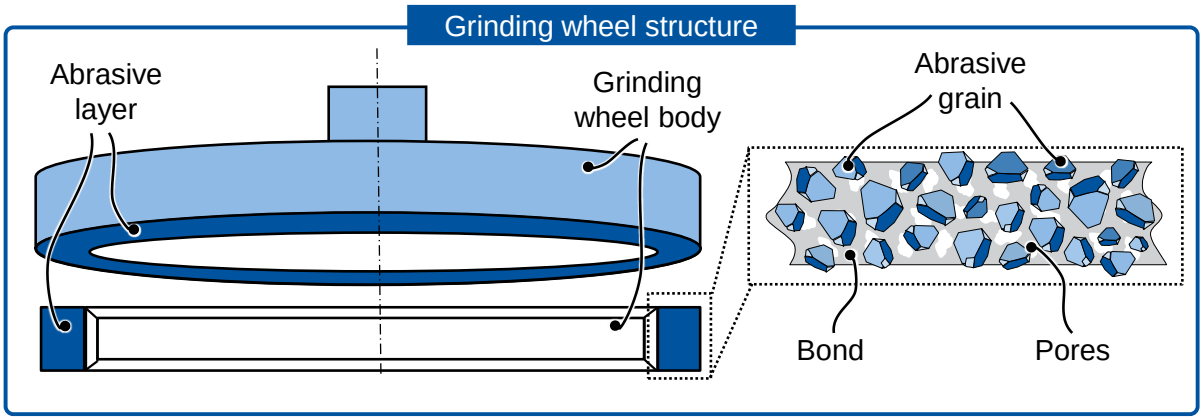

Figure 2.14: Structure of a grinding wheel

Material removal mechanism

Understanding the mechanism of material removal is crucial to cope with the grinding process. Thanks to a series of operations and the contribution of the cutting-edge form, material is removed followed by different phases depending on the type of material that is being grinded. Consequently, two mechanisms can be observed as ductile and brittle behavior. Both of them are divided in three phases.

Grinding ductile materials

Figure 2.15.a shows the first phase of ductile materials grinding. This first phase is based on elastic deformation thanks to the cutting edge. This edge penetrates the workpiece on a flat path. Subsequently, a second phase occurs with the plastic deformation of the material previously deformed. Finally, the chip formation happens when the cutting edge has penetrated enough so that the chip thickness h_{cu} corresponds to the grain cutting depth $T\mu$ [KLOC09, p. 9].

Grinding brittle materials

Figure 2.15.b shows the first phase of brittle materials grinding. This phase is exactly the same as in brittle materials. A second phase of elastic and plastic deformation follows but, in this case, is of very short duration due to the mechanical behavior of the material. Moreover, at the same time micro-cracking starts. Finally, the chip formation starts when the depth of cut h_{cu} overcomes the critical depth of cut $h_{cu,krit}$. Consequently, radial and lateral cracks occur which lead to spalling and damage of the surface [KLOC09, p. 9].

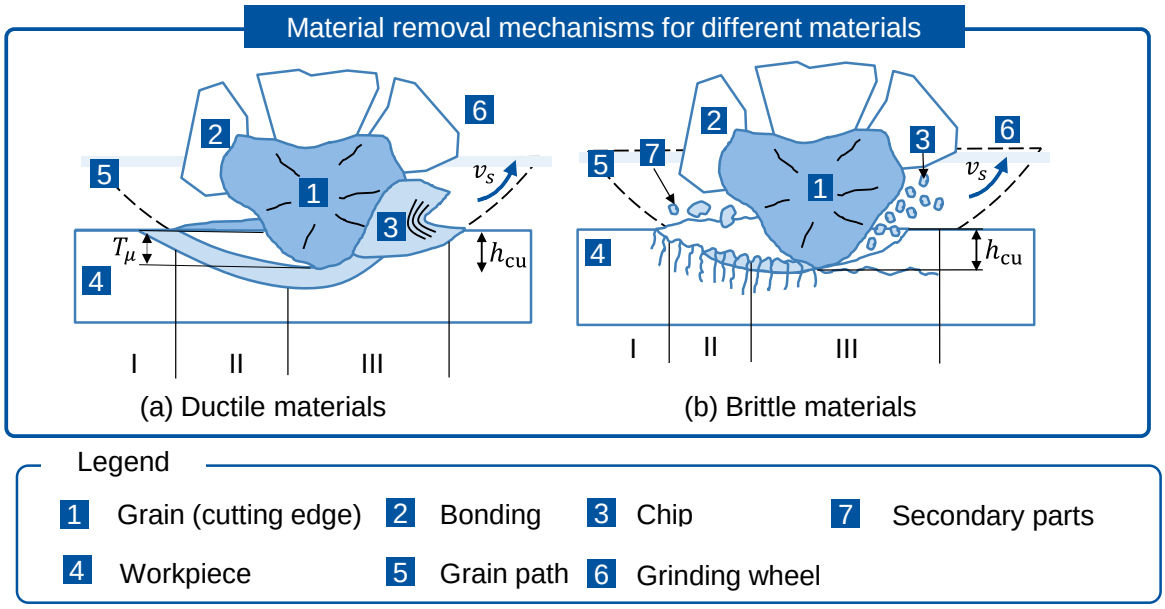

Figure 2.15: Material removal mechanisms for different materials [KLOC09]

2.3.3 Intermediate conclusion

Grinding is a manufacturing process classified under the category of cutting with geometrically undefined cutting edges. In particular, the technique studied is defined as longitudinal side - face grinding. This process is applied for obtaining accurate tolerances such as complete leveled surfaces. For this purpose, a grinding tool is necessary which is composed by the base body and abrasive material. On one side, the grinding wheel body or base body. This component is the main frame where the abrasive coating is held. On the other side, the abrasive material is the composition of grit materials and binder. These components are responsible for providing proper mechanical and thermal properties to the grinding wheel. In addition, grit materials are responsible for providing the abrasives properties. Also, they are classified by synthetic such as cBN or silicon carbide, or natural such as corundum or diamond. In contrast, bond materials are responsible for keeping together the grit material to the frame. There are types as resin, vitrified or metallic. Moreover, depending on the material, which is bonded to, is possible to find pores in the abrasive coating depending on the grit material applied.

Chip formation is a significant step while grinding due to its high influence on material removal. For that purpose, there are two possibilities of chip formation depending on the material which is grinded. On one hand, grinding on ductile materials is based on elastic deformation, plastic deformation and chip formation. On the other hand, grinding on brittle materials is divided in three phases as well. In this case first and second phase are similar, but at the end of the second phase microcracks occur which result with a chip formation. This chip formation ends up with surface damage and spalling. This field of study is still on developing due to its high complexity.

2.4 Current trends on simulation

Machining is one of the major manufacturing processes in industrial production and it plays an important role in modern industry [AGME18, p. 2853]. Therefore, simulation of this manufacturing processes has become an essential technique for planning and improving processes. In almost all manufacturing processes (e.g. forming, cutting, grinding etc.) simulation is an important tool which assists the engineer in tasks such as designing,

optimizing or controlling processes. Furthermore, these tools help to understand and predict fundamental mechanisms during the series of operations. In this section the most common simulation methodologies such as molecular dynamics, finite element analysis, regression analysis, artificial neural networks and rule-based approaches will be reviewed. The section presents a description of the main simulation methodologies followed by their definitions, applications and a comparison between their advantages and drawbacks.

Molecular dynamics

Molecular dynamics (MD) is a numerical method describing the lattice constants and orientation, chemical elements, and the atomic interaction. Regarding grinding, it is commonly used for removal processes at the atomic or nanometer level [RENT14]. Figure 2.16 shows all the components previously mentioned, including their mutual interactions. The main field of application of this simulation process is ultra-precision machining applied to microelectronics, optics or micromechanics [LI18, p. 1].

The main drawbacks are presented subsequently. Firstly, the application in real size models including the interaction between all the elements involved is limited, because of numerous variables such as number of atoms or process observation time that do not allow bigger models. Moreover, the lack of potential functions that explain the interactions of typical engineering materials are another fact that limits the application of this tools [RENT14]. As a result of that, heavy CPU-power is needed in order to achieve results. Finally, the actual state of the art in MD grinding, scratching or cutting does not consider fluids and there is a lack of experimental validations in this area [RENT09, p. 24].

In contrast, one main advantage of this tool is the large 3D atomistic model and detailed comprehensive representation of solids as well as amorphous materials or polymers. Material properties such as plasticity, elasticity, brittleness or ductility are profoundly treated. Furthermore, atomic contact, friction, fracture and plastic deformation are considered. Therefore, it provides a deep theoretical insight into cutting processes on a nanometer level which cannot be achieved through experimentation [RENT09, p. 23]. Thus, this fact makes MD the best way to investigate the nanometric cutting processes [LI18, p. 2]. Finally, this kind of software is helpful regarding work with other models which can lead to interesting thermomechanical behavior prediction.

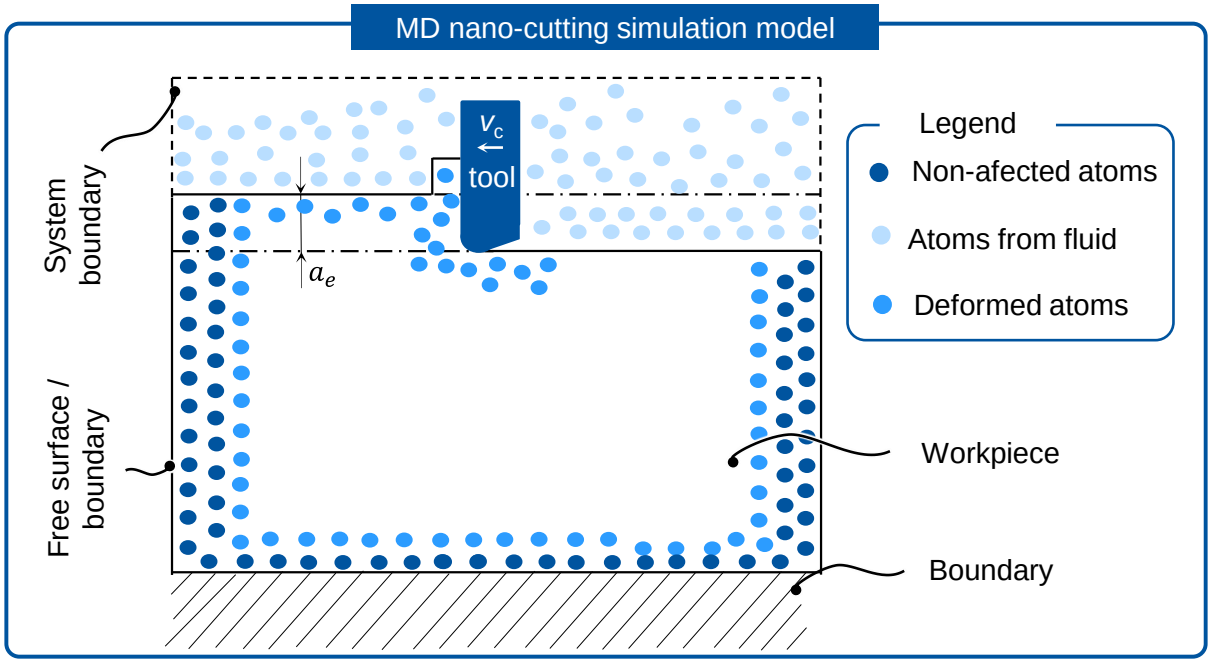

Figure 2.16: Graphic example of the application of molecular dynamics [RENT14]

Finite element analysis

Finite Element Method (FEM) is a numerical method used to approximate the solution of boundary- and initial-value problems characterized by partial equations [TEKK14, p. 508]. Moreover, as reported by Klocke, Finite Element Analysis (FEA) is the application of FEM into a process by approximating continuous functions to discrete models [KLOC11, p. 197]. This methodology is applied in numerous fields such as structural mechanics, thermodynamics or fluid mechanics, but more interest is given in cutting processes due to the nature of this work such as drilling, milling, turning, and planning. Furthermore, special interest among the scientific community is centered on analyzing chip formation in cutting processes by applying this kind of techniques [DUCO19, p. 143].

As stated by several authors, the continuous functions use Eulerian and Lagrangian approach. On one hand, Eulerian formulation states that the mesh is fixed in space and the material flows through it. Thus, the mesh remains undeformed (figure 2.16.a). Conversely, in the Lagrangian formulation the mesh is attached to the material, so it follows with a large deformation (figure 2.16.b). In order to apply Eulerian formulation , knowledge about chip geometry and chip tool contact is previously required, while in Lagrangian formulation the main problem is the excessive distortion in the mesh due to large deformations. A solution that deals the best with these problems is defined as Coupled Eulerian-Lagrangian (CEL), which is an application of both formulations. Herein, the workpiece is modelled with Eulerian formulation and the tool is described by Lagrangian formulation [DUCO19, p. 143].

Some advantages of this technique are presented in the following. Primarily, the user does not need to be highly skilled and experienced in order to use the software based on this principle where it is possible to add numerous features related to micro- and macro-thermomechanical properties as well as processes such as friction, wear or heat generation. Moreover, it has high transferability among a huge variety of programs that allows further research under specific topics. Finally, these techniques are characterized by a high flexibility in different fields of application as earlier mentioned.

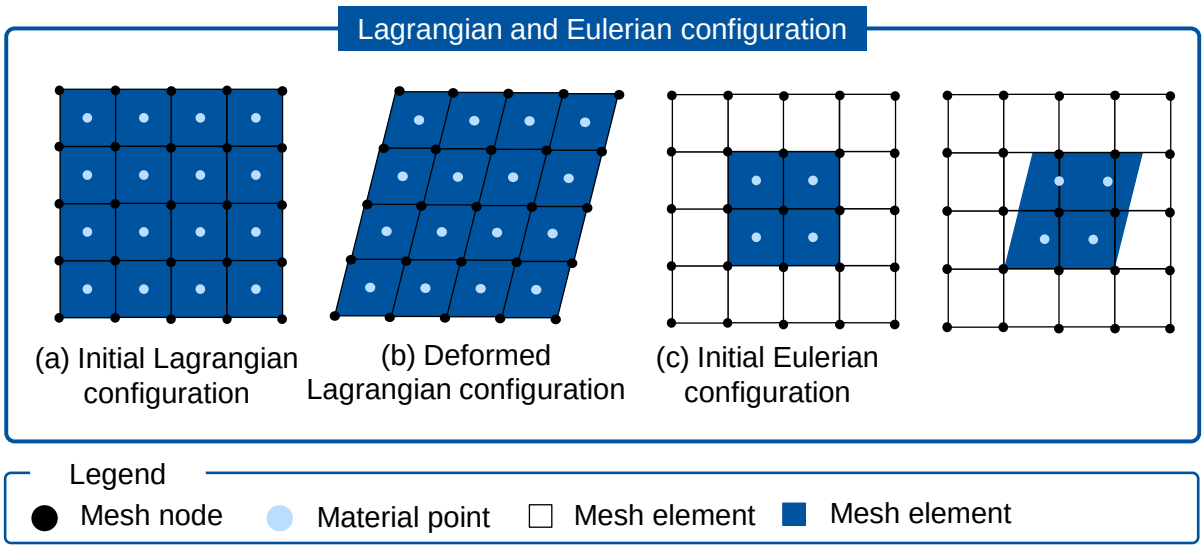

Figure 2.17: Difference between Lagrangian and Eulerian mesh configuration

In contrast, the main drawbacks are shown subsequently. First of all, huge CPU-power is demanded when applying modifications to the model leading to long computation times. Subsequently, since this approach allows to show specific details of the processes, generally it is a complicated procedure, and it demands high effort in order to conduct experiments

and data analysis. Finally, as commented earlier, due to the high complexity of FEM models, it is common to find that the software is asking for properties that are not available in the bibliography. Therefore, this fact limits the possibility of developing deeper knowledge of the model.

Regression analysis

Regression analysis (RA) is a statistical technique for modeling the relationship between a dependent variable and one or more independent variables. Dependent variables are modeled as a function of independent variables related to coefficients (regression parameters $\beta_0, \beta_1, \beta_2, \dots, \beta_n$) and a random error term (ϵ). In order to get this regression model done, a database has to be developed by doing machining experiments, although current trends utilize linear regression or back propagation algorithms to obtain these data [CHIL00, p. 267]. Moreover, this simulation process is classified in linear regression, multiple linear regression and non-linear regression.

More attention is given to non-linear system for cutting forces (H), as shown in equation 2.19, where $F^T = \{F_d, F_f, F_c\}$ represents the cutting forces vector, and $x^T = \{V, f, d\}$ are the operation variables [CHIL00, p. 267]. Constants in regression *K* are substituted.

$$F = H(x) \quad \textbf{(2.19)}$$

$$F_{\mathrm{d}} = K_1 \cdot f^{0.46} d^{0.81} + K_2 \cdot (VS^{1.93} - K_3 \cdot lnV) \cdot (VB^{0.26} - K_3 \cdot lnV) \cdot \ (VN^{-0.33} - K_3 \cdot lnV) \quad \textbf{(2.20)}$$

$$F_{\mathrm{f}} = K_4 \cdot f^{0.3} d^{0.72} + K_5 \cdot (VS^{3.58} - K_6 \cdot V^{0.27}) \cdot (VB^{-0.66} - K_7 \cdot V^{0.27}) \cdot \ (VN^{0.03} - K_7 \cdot V^{0.27}) \quad \textbf{(2.21)}$$

$$F_{\mathrm{c}} = K_9 \cdot f^{0.94} d^{1.11} + K_{10} \cdot (VS^{0.24} - K_{11} \cdot lnV) \cdot (VB^{0.23} - K_{11} \cdot lnV) \cdot \ (VN^{0.16} - K_{11} \cdot lnV) \quad \textbf{(2.22)}$$

As shown in equations 2.20, 2.21., and 2.22, this non-linear system is not trivial to analyze since, despite the presence of linear and previously known equations, the dynamical behavior of some equations is complex and composed by numerous variables. Thus, a non-linear regression matrix H_{R} is used with the aim of finding the solution in this case.

The possible applications of this tool are numerous fields such as biology, agriculture or economics, but more interest is given on engineering and its use in cutting processes due to the nature of this work [YAN05, p.3].

The main advantages are the following. Firstly, since this simulation process is model-based, this fact helps to diagnose and monitor the cutting state problems in complicated machining problems. Moreover, global optimization is easier to apply thanks to this model-based nature [CHILD00, p .320]. Secondly, thanks to the previous work done related to developing the model and obtaining the database, the computational power needed is not very high. Finally, as mentioned in the first paragraph, RA is an empirical analysis which is suitable for numerous subjects and areas due to its flexibility and versatility.

Finally, the main RAs drawbacks are explained hereafter. First of all, as commented earlier, the model and database need to be done before the simulation. Therefore, these tasks increase the time and complexity of the use of this technique [YAN05, p. 5]. Consequently, previous deep knowledge and understanding in the fields of statistics and mathematical analysis narrows the application of this field mostly on research. Finally, since the database is sustained by the number of experiments, simulation process time and data quality increase the complexity and time of this simulation.

Artificial neural nets

Artificial neural networks (ANN), usually called neural networks (NN), are a soft computing method that consists of a mathematical model or computational model based on an adaptative system that changes its structure based on external or internal information that flows through the network. They are usually applied to model complex relationships between inputs and outputs or find patterns in data as is shown in figure 2.18 [DADD14, p. 911]. This fact makes this kind of empirical models an easy way to infer a mathematical function from observations.

According to D'Addona, main applications are system identification and control (vehicle control, process control), data analytics, pattern recognition or decision making among others [DADD14, p. 917]. Moreover, Cheng et al. reported its application in chatter during machining [CHEN09, p. 127], and Moriwaki and Mori used it for pattern recognition in order to make a classification of cutting states during turning S45C carbon steel [CHIL00, p. 310]. Nevertheless, as reported by Brinksmeier et al., possible applications to grinding exists for the prediction of grinding output parameters such as surface roughness, grinding forces and the prediction of optimal input parameters at which desired output parameters are achieved, and grinding monitoring in order to predict unfavorable phenomena [BRINK06, p. 684].

As reported by Brinksmeier et al, the main advantages of ANNs applied to model grinding processes are subsequently explained. Firstly, the automated construction of a nonlinear model of observed phenomena and an automated fusion of information from various sensors is useful in order to apply it. In addition, thanks to the simplicity of these models to manage soft input parameters, i.e. parameters without numerical values, such as coolant type or nozzle type and the possibility to inter- and extrapolate values, helps to adapt this tool to different manufacturing processes. Lastly, thanks to the flexibility of this simulation model, one great advantage of this model is the possibility of combining it with other models [BRIN06, p. 688].

Finally, the main drawbacks are presented. Firstly, the correct and precise selection of representative signals for posterior processing is a complex task that is possibly a source of problems considering the huge quantity of parameters that influence the grinding process [BRIN06, p. 684]. Furthermore, since this model also relies on a previous dataset and quality of observed data, longer simulation time and complexity are expected. In addition, the choice of learning algorithm requires numerous experiments in order to tune and train all the data, which tends to be a problem [DADD14, p. 915]. Finally, another disadvantage of this technique is the poor acceptance among users and, therefore, use in industry. This fact is based on the lack of transparency of the data stored inside the ANN and huge effort for correct development of the neural network [BRIN06, p. 687].

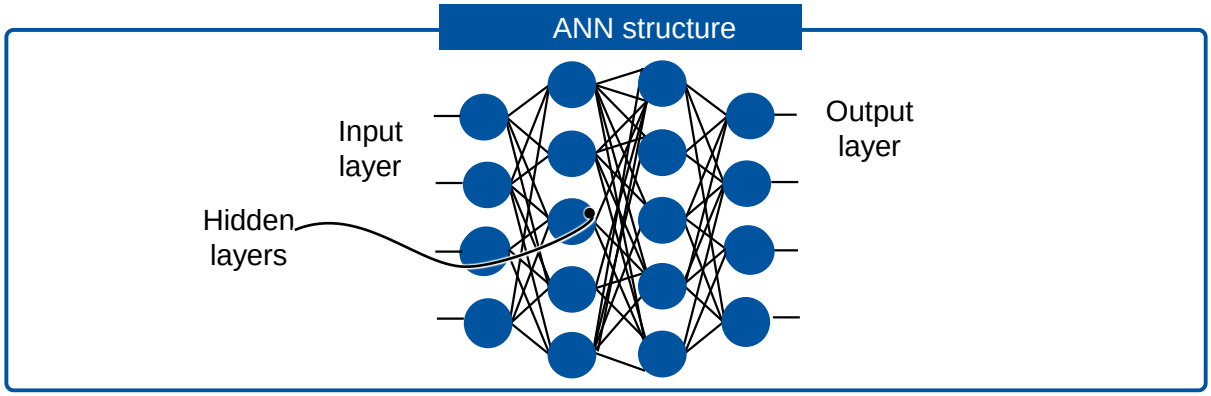

Figure 2.18: Structure and parts of artificial neural networks [CHEN09, p. 127]

Rule based processing approach

Within the field of grinding processes there are different approaches related to artificial intelligence. In these kind of techniques rules used to teach the system how it should work are described by the programmer in such a way that the performance of this model is goal-oriented and structured by a “feedforward control” through a stored rule [RASM83, p. 258]. The particular methodologies which are applied in the field of grinding related to this topic are fuzzy logics (FL). This methodology is defined as an extension and generalization of classical multivalued logics [CAGG14, p. 562]. This system is designed to handle partial truth (extension of the ordinary set theory with values between 0 and 1) using membership functions (MFs). These MFs are curves characterizing how each point of the input space is mapped to a membership value (degree of membership or truth degree) [CAGG14, p. 563]. Accordingly, there are values between 0 and 1 to characterize the fuzzy members as it appears in figure 2.19 [BRIN06, p. 684].

As reported by Caggiano, FL models are mainly used in decision-making process, robotics, pattern classification, control or manufacturing. More attention is given to some grinding utilization of these models in collaboration with neural networks [CAGG14, p. 601].

Subsequently, the main advantages of FL models are shown. Firstly, this system has the capability to take knowledge based on human experience and the possibility to model human reasoning, especially with problems with a lot of input parameters [BRIN06, p. 686]. This fact is helpful to simplify the model. Moreover, it has the advantage of higher capability with less CPU power compared to empirical models. Secondly, another competitive advantage compared to other models previously mentioned is the absence of datasets to start working. Furthermore, it has specificized field dedicated characteristics related to the MF that allow for better performance than other modelling tools [CAGG14, p.563]. Finally, as commented before, these models are easy to combine with NN to obtain greater quality data from them.

Conversely, the main drawbacks are the following. Firstly, sophisticated knowledge is demanded as the complexity related to basic knowledge and effort in experiments is very high. Furthermore, although the quality of the outcome data is high, the ability to switch to other grinding application is narrower. Therefore, it reduces the versatility compared to other simulation models. Finally, the last drawback of this process is the high maintenance and further development requirements in order to keep these simulation models updated [BRIN06, p. 687].

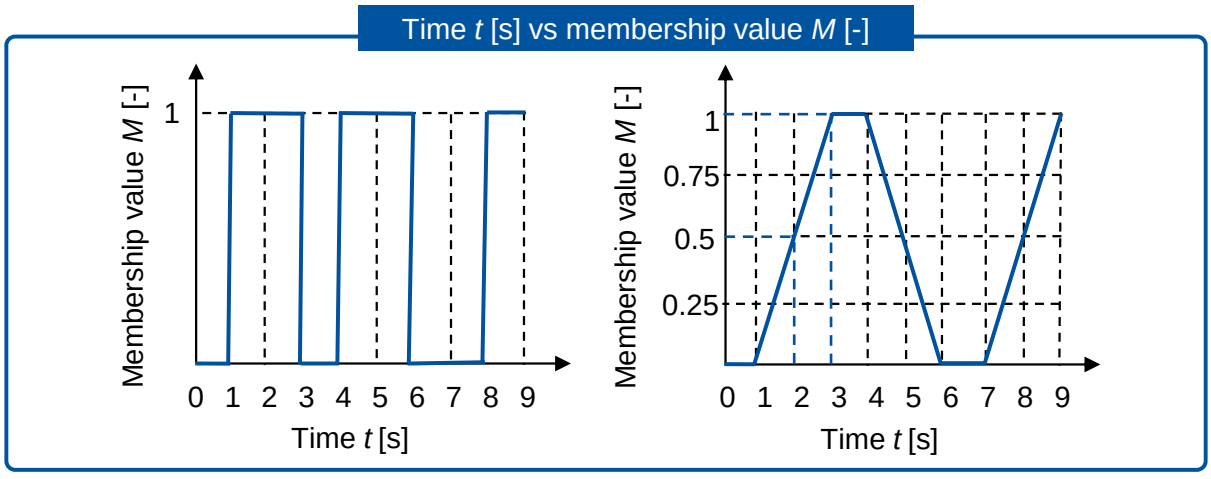

Figure 2.19: Effect of time *t* [s] with respect of membership value *M* [-] [BRIN06]

2.4.1 Intermediate conclusion

Simulation supposes a significant tool in order to study any manufacturing process by predicting the possible outcome. For that purpose, four simulation methodologies were MD,

FEA, RA and ANN. First of all, MD are used for describing micromechanical and thermodynamic properties of a sample volume. The advantages of this method are the atomistic structure design, significant material properties and the possibility of making nanometric simulations. In contrast, the main drawbacks are their limited application, noticeable power needed, and liquids are not possible to model. Then, FEA is the application of FEM into a process of approximating continuous functions to discrete models. The advantages of this method are the low skills needed, high transferability among programs and high flexibility related to the process to simulate. On the other hand, the main drawbacks are significant CPU times when complex process are simulated, properties unknown or difficult to find in the literature and high complexity to transfer the simulated data into real experiments. In contrast, RA is a statistical technique for modeling the relationship between a dependent variable and one or more independent variables. The main advantages are low computational power, high flexibility among different disciplines and easiness to diagnose and monitor the cutting state problems. In contrary, a model database needs to be developed, extensive knowledge in statistics and mathematics needs to be known and there is a heavy dependence on database in regard to the outcome of quality results and simulation time. Finally, ANN are mathematical models that changes its structure based on external or internal information that flows through its network. The main advantages are the possibility of building non-linear models with merged information, huge capacity to manage numerous input variables and flexibility of this simulation software that allows to apply it in several fields. In contrast, the main drawbacks are the dependency of the quality of the dataset, the high complexity of this method and the choice of the algorithm to train the data. Therefore, depending on the expected outcome, the available knowledge and the budget, these tools are possible to be chosen.

3 Economic and scientific problem

The central motivation of this work lies on two problems. On one hand, the atomic structure transformation of diamond into graphite at high temperature and the low hardness H_V of resulting graphite. Consequently, a diamond grinding wheel will lose its ability to grind in case it reaches those temperatures. On the other hand, the measurement of the maximum temperature on individual abrasive grains in the grinding process is not possible due to the uncertainty while measuring temperature. In particular, the pyrometer is the measuring instrument responsible for this task. This device has a diameter d_{pyro} = 800 µm and the diameter of a diamond grain d_g = 15 µm. This gap on size supposes that there are several diamonds in contact with the pyrometer at the same. Moreover, this gap is also surrounded by coolant oil and chips generated. Consequently, there is not a homogeneous temperature to measure. Finally, the pyrometer measures the radiation of the surface. For that purpose, it recalculates the temperature by a coefficient of emission with the actual measured radiation of the surface, but, since the temperature is not homogeneous enough, it is not possible to precisely calculate the coefficient of emission. There is no measuring device that provides maximum temperature.

Therefore, simulations are conducted based on a finite element model. This simulation enables to predict the maximum temperature and heat distribution during grinding in PCD and pcBN workpiece. Both the maximum temperatures and heat distribution in the contact zone A_W are achieved depending on the tribological input variables.

Achievable benefits are mentioned in the following thanks to these simulation results. Increasement of grinding wheel tool-life due to wear reduction. Optimization of grinding process design where diamond and pcBN are involved. Minimization of maintenance. Consequently, all these possible benefits could lead to cost reduction and economical profitability.

For a knowledge-based process design, the cause and effect-relationships in the pcBN heat transfer process must be explained, the tribological conditions in the contact zone A_W understood, material properties and boundary conditions properly defined. This includes knowledge of the interaction between the tribological input variables, the thermal loads in the contact zone A_W and the surfaces of the active partners that change over time. Furthermore, mathematical approaches based on tribological and grinding parameters in PCD CMX850 are applied. Consequently, the maximum temperature and heat distribution in the contact zone A_W during pcBN grinding is obtained. Moreover, experimental data is used to compare these simulation results with pcBN simulations. For this reason, the prediction of the resulting maximum temperature and heat distribution in the workpiece will be possible.

Based on these findings, the following research hypothesis is formulated:

The single grain temperature in the contact zone during grinding different pcBN specifications can be predicted with a simulation model as a function of the tribological input variables, material properties and boundary conditions applying an empirical-analytical thermal model.

The following research objective is pursued:

The aim of this thesis is to develop a simulation model that provides the temperature of single grains during surface grinding in the workpiece contact zone for different pcBN specifications.

To achieve the research goal, the following research questions are formulated:

Research question 1: How can the empirical-analytical model from PCD be applied to pcBN?

Research question 2: How much differs the heat transfer mechanism between PCD and pcBN?

Research question 3: How much does the workpiece microstructure influence the heat distribution and maximum temperature on the contact zone?

Research question 4: How can temperature and heat distribution during grinding of different pcBN specifications be predicted with a FE model?

In order to answer research questions number 1 and 2, chapter 5 analyzes a simulation model from the PCD CMX850 workpiece. Also, material properties are modified by applying pcBN properties taking from the literature. For that purpose, material properties, boundary conditions and thermal load will be examined. In particular, the thermal load will be studied in order to extensively understand the empirical-analytical model applied in the PCD CMX850 workpiece.

Research question 3 is answered in chapter 6. This chapter develops a new model based on material properties and boundary conditions proposed by Vits. Nevertheless, 3D geometry is totally modified where random distributed grains and binder are modelled in a different approach. Furthermore, experimental data from is used as an input for thermal load.

Finally, research question 4 is discussed throughout both chapters previously mentioned. On one hand, chapter 5 compares maximum temperature and heat distribution of PCD CMX850 in comparison with pcBN specifications as DBW85, DCN450 and DCX650. On the other hand, maximum temperature and heat distribution results of pcBN DBW85 is discussed in further detail.

4 Research methodology

Figure 4.1 shows the general research methodology developed throughout this study. This graph explains the procedure to verify the research questions by steps. First, all the material properties and mathematical formulation such as grinding power P_c or Heat Flux Load *HFL* is collected. Experimental results for discussion are gathered as well. Secondly, the 3D geometry is created in phase two. All the geometrical characteristics to simulate are stablished. At this point, next phase is enabled because both requirements are compulsory in order to reach next step. Therefore, the simulation is executed according to boundary conditions. Also the geometrical part imported from the designing software is meshed. After, the simulation results are achieved. These results are compared and discussed with experimental results previously gathered. In subsequent chapters this methodology is explained in more detail.

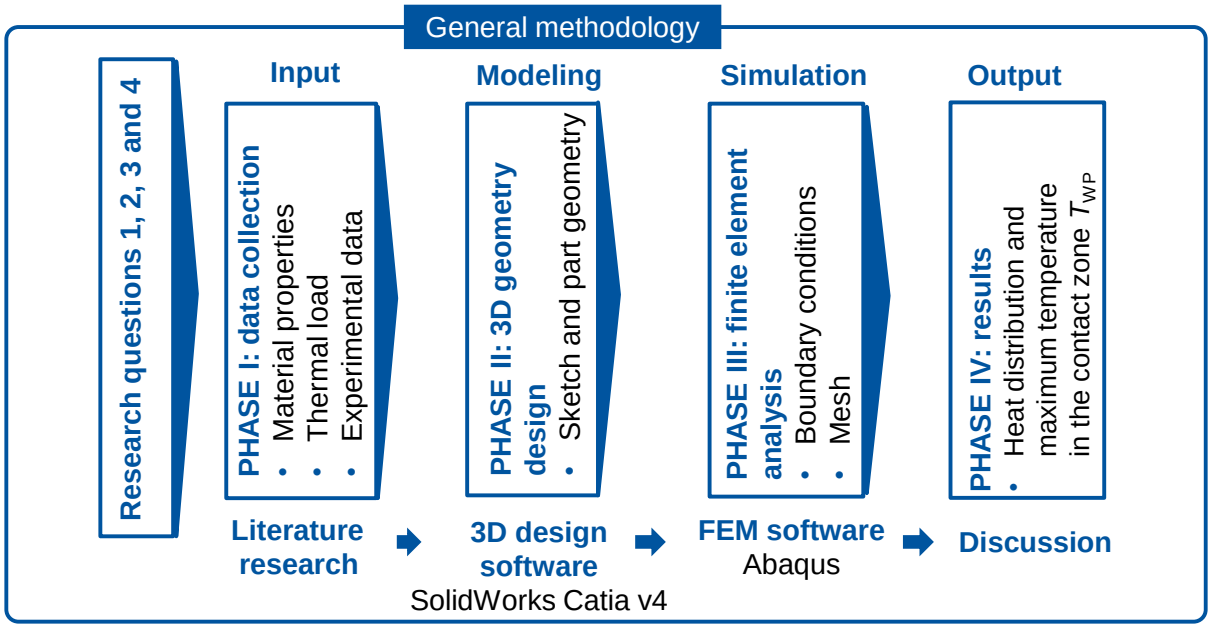

Figure 4.1: General methodology of simulation for single grain temperature of pcBN and PCD grinding

5 Finite element simulation of the thermal load during PCD and pcBN grinding

Thermal load on individual abrasive grains during pcBN grinding is not yet possible to measure with the actual measurement technology. Therefore, accurate simulations should be conducted in order to understand the heat transfer process. In this case, a simulation model based on Vits work is explained below. The definition of material properties of PCD CMX850 and pcBN DBW85, DCN 450 and DCX650 are presented first (section 4.1), followed by the description of the simulation model (section 4.2). Finally, the results of the simulations are compared and analyzed at the end (section 4.3).

5.1 Methods and materials

Figure 5.1 presents the research methodology stablished to develop this simulation model. This method is an implementation of the one presented in chapter 4. In particular, this technique provides answers to research questions 1, 2 and 4. In this chapter more focus is concentrated in the first two ones. For that purpose, this process is divided in four stages. Phase I is presented in subsections 5.1.1 and 5.1.2 with all the material collected from the literature revies. Then, phases II and III are explained in subsection 5.1.3. All the specifications about the geometrical and simulation model are presented. Subsequently, results achieved are shown in section 5.2 and then discussed in section 5.3.

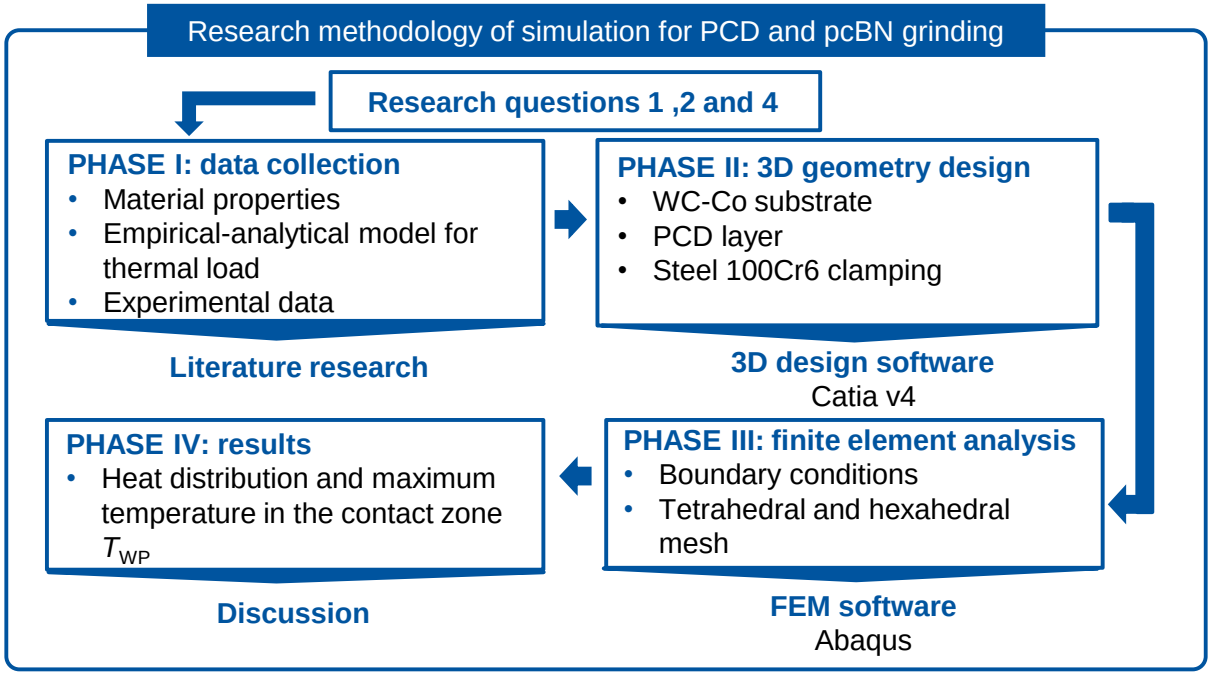

Figure 5.1: Research methodology of simulation for single grain temperature on pcBN and PCD grinding

5.1.1 Determination of material data

Mechanical and thermal properties are crucial during the previous steps before running the simulation due to their heavy influence on the results. The thermophysical properties of PCD, pcBN and binder materials such as cobalt or AlWCoB were taken from the literature. These properties are presented throughout this chapter. Furthermore, all these materials were considered as temperature-dependent, isotropic and elastic material behavior without

chip formation [VITS20, p. 91]. Although it is possible to make anisotropic and brittle material behavior, high computing capacity it is needed.

The 3D model geometry is composed by 4 components. A part of the PCD CMX850 workpiece where the grains are considered, a substrate made of Cobalt and 2 steel 100Cr6 (steel for rolling bearings) blocks that mimics the clamping into the machine. Both the 1 mm thick hard metal substrate and the 0.6 mm thick PCD layer were taken into account. Table 5.1 shows material properties applied into this geometry.

Table 5.1: Material properties for simulation

Material property	Symbol	Unit	c-BN	CMX850	100Cr6[g]	Cobalt[g]	DBW85	DCX650	DCN450	AlWCoB
c-BN content	*w*	%	-	85[g]	-	-	85[a]	65[a]	45[a]	-
Binder/Matrix	-	-	-	Co[g]	-	-	AlWCoB[a]	TiN	TiCN	-
Conductivity	λ	W/m·K	1300[d]	253.5[h]	32	80	87.5[a]	52.6[a]	32.8[a]	8.7[j]
Density	ρ	kg/m^3	3450[f]	4300[g]	7800	14900	3107[b]	3037[b]	2971[e]	2537[k]
Poisson's ratio	*v*	-	0.16[i]	0.08[g]	0.3	0.22	0.191[c]	0.191[c]	0.191[c]	0.251[l]
Young Modulus	*E*	GPa	605[i]	15.5[h]	210	630	4.9[a]	5.5[a]	2.9[a]	370[l]
Facture toughness	K_{Ic}	Mpa·m$^{0.5}$	-	827[g]	-	-	574[a]	620[a]	646[a]	-
Specific heat (T = 25°C)	c_p	J/kg·K	510[d]	536[b]	460	167	1020[d]	1103.34[b]	1170[b]	61.882[m]

[a] [MULL21, p. 1150], [b] Value obtained from figure 5.2, [c] [PROE18, p. 538], [d] [MORG98, , p. 664], [e] [LI20, p. 571], [f] [TAN90, p. 21], [g] [VITS20, p. 157], [h] [VITS20, p. 48], [i] [JIAN03, , p. 1516], [j] [QUES09, p. 157], [k] [ECKE71, p. 2], [l] [YAO16, p. 4], [m] [YAO16, p. 7]

Since it was not possible to find the density values for DCN450 and DCX650, figure 5.2 was done. This graphic represents a regression over the density values from [LI20, p. 20]. Consequently, the linear equation resulted from this linear approximation is presented in the following.

$$\rho(w_{\mathrm{c-BN}}) = 0{,}0035 \cdot w_{\mathrm{c-BN}} + 2{,}8102 \qquad \textbf{(4.1)}$$

Therefore, applying equation 4.1 for values of 85% (DBW85) and 65% (DCX650) of c-BN, the values obtained are:

$$\rho_{\mathrm{DCX650}} = 0{,}0035 \cdot (65) + 2{,}8102 = 3.037{,}7 \frac{\mathrm{kg}}{\mathrm{m}^3}$$

$$\rho_{\mathrm{DCN450}} = 0{,}0035 \cdot (85) + 2{,}8102 = 3.107{,}7 \frac{\mathrm{kg}}{\mathrm{m}^3}$$

Similar process was done with the aim of finding the specific heat c_p for values of 85% (DBW85) and 65% (DCX650) of c-BN. For that purpose, knowing previously values from [MORG98, p.664] shown in figure 5.2 and it resulted linear approximation showed below.

$$c_p(w_{\mathrm{c-BN}}) = -3{,}333 \cdot w_{\mathrm{c-BN}} + 1.320 \qquad \textbf{(4.2)}$$

By applying the aforementioned equation, specific heat c_p obtained are the following.

$$c_{p\,\mathrm{DCN450}} = -3{,}333 \cdot (45) + 1.320 = 1170 \ \frac{\mathrm{J}}{\mathrm{kg} \cdot \mathrm{K}}$$

$$c_{\mathrm{p\ DCN450}} = -3{,}333 \cdot (65) + 1.320 = 1103{,}34\ \frac{\mathrm{J}}{\mathrm{kg} \cdot \mathrm{K}}$$

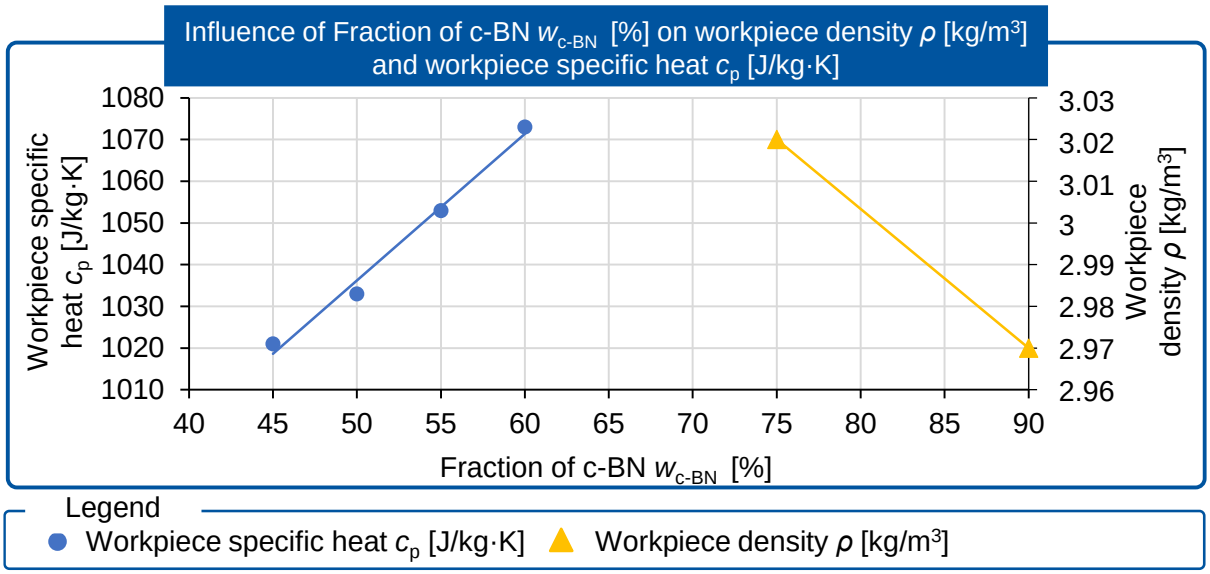

Figure 5.2: Graph about the influence of fraction of c-BN $w_{c\text{-}BN}$ [%] on workpiece density ρ [kg/m³] [LI20, p. 571] and workpiece specific heat c_p [J/kg·K] [MORG98, p. 664]

5.1.2 Thermal load calculation

The aim of the developed finite element model was to calculate the maximum temperatures in the Contact zones of individual abrasive grains in the workpiece for pcBN and PCD specifications taken into account results from VITS (stage 1 and stage 2.2 simulations). Consequently it is possible to understand the difference in heat transfer mechanisms between both pcBN and PCD specification. For that purpose, mathematical models used by VITS were used with the aim of modeling experimental data and material properties into a heat load. This heat load is defined in the finite element software as Heat Flux Load (HFL) and it was calculated applying the following equation [VITS20, p. 76].

$$P_{\mathrm{C}}(F_n, K_{\mathrm{lc}}, v_{\mathrm{s}}) = k_{\mathrm{KSS}} \cdot k_{\mathrm{sls}} \cdot v_{\mathrm{s}} \cdot (-0.0147 \cdot k_{\mathrm{ic}} + 1.3481) \cdot (3 \cdot 10^{-6} \cdot F_{\mathrm{n}}^3 - 3 \cdot 10^{-6} \cdot F_{\mathrm{n}}^2 + 0.1053 \cdot F_{\mathrm{n}}) \quad \textbf{(4.3)}$$

Table 5.2 presents parameters from experiments done by Vits. This data was applied in equation 4.3 with material properties were provided in section 5.1.1. This resulted in grinding power P_c. Consequently, the heat source was simulated on the assumption that 85% of the cutting power P_c is converted into heat. This assumption is based on measurements about grinding tests. This fact based on the stage 1 simulations enables to transfer the cutting power P_c into the heat flux load *HFL* [VITS20, p. 90]. Furthermore, these simulations demonstrated that 93.2% of the whole heat load was transferred into the workpiece and the residual 6.8% was dissipated through the grinding layer.

Once the grinding power P_C was calculated considering all previous assumptions from VITS stage 1 simulations, these results were divided by the grinding area A_W = 0.495 mm² in order to achieve the appropriate units which are demanded from the software ($J \cdot T^{-1} \cdot L^{-2}$). The reason for using this value is based on the cross-sectional area between the abrasive grain of the grinding wheel which contact the workpiece only in certain spots which is only a fraction of the wheel surface area.

Table 5.2: Experimental data description

Experiment number	Depth of cut a_e [µm]	Grinding wheel speed v_s [m/s]	Feed rate speed v_w [m/min]	Normal force F_n [N]
1	1	20	150	90.705
2	5	10	150	108.66
3	5	20	150	129.935
4	5	30	150	119.225
5	9	20	150	157.995

As a result of these reasons, the heat flux load *HFL* can be summarize by applying equation 4.4. Consequently, heat flux load *HFL* values are different among the chosen material specification as it is proven in the table 5.3.

$$HFL(F_n, K_{Ic}, v_s, A_w) = 0.85 \cdot 0.938 \cdot (-0.0147 \cdot K_{ic} + 1.3481) \cdot \frac{A(F_n)}{A_w} \quad \textbf{(4.4)}$$

$$A(F_n) = (3 \cdot 10^{-6} \cdot F_n^3 - 3 \cdot 10^{-6} \cdot F_n^2 + 0.1053 \cdot F_n)$$

Table 5.3: Heat flux load for different materials

Experiment number	Heat flux load for CMX850 HFL_{CMX850} [W/mm²]	Heat flux load for DBW85 HFL_{DBW85} [W/mm²]	Heat flux load for DCN450 HFL_{DCN450} [W/mm²]	Heat flux load for DCX650 HFL_{DCX650} [W/mm²]
1	331.39	377.48	386.18	374.87
2	208.57	237.58	243.06	235.94
3	539.05	614.03	628.18	609.79
4	711.88	810.9	829.58	805.29
5	743.52	846.94	866.46	841.09

5.1.3 Structure of the finite element model

The simulation model was build based on the material assumptions previously explained. These properties were Young modulus *E*, Poisson's ratio *v*, density *ρ*, thermal conductivity *λ*, fracture toughness K_{Ic} and specific heat capacity c_p. Likewise, boundary conditions explained throughout this section were stablished by Vits [VITS20, p. 92].

First of all, the heat sources on the workpiece surface calculated according to equation 4.4 and presented in figure 5.3 were not moved, because friction models applied in Abaqus highly increase the simulation time t_{sim}. This measure represents a simplification of the real contact conditions which made a reasonable simulation time t_{sim}. On the other hand, the heat flux load *HFL* was applied according to a specific amount of time based on a tabular table in order to control the fraction of heat flux load *HFL* applied. Furthermore, these values shown in table 4.8 are linked to the step where the heat load is stablished. Consequently, the heat flux load HFL follows the function wrote in the tabular table from figure 4.3. In this case the time stablished for the heat flux load *HFL* defined in the step load was t_{step} = 10 s.

Heat transfer by convection to the Sintogrind TTK grinding oil was taken into account in the areas between the grain Contact zones. All other surfaces of the abrasive coating were assumed adiabatic. Furthermore, the heat flow that goes into the workpiece has a constant heat load and no time to cool down because there is no stop during the whole experiment. Therefore, the workpiece is constantly receiving heat. On the other hand, the grinding wheel is cooled down, because the contact area between the grinding wheel and workpiece differs since the grinding wheel is rotating according grinding wheel speed v_s. Moreover, a uniform temperature distribution of T = 25°C was considered among all the bodies in the simulation model. Finally, no mechanical boundary conditions were assumed since this model only considered the thermal loads, except tying constrains between 3D parts of the model.

Time *t* [s] *vs* Amplitude value A_v [-]

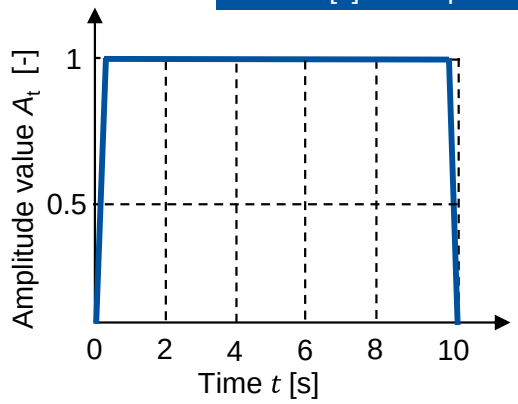

Amplitude value A_t [-]	Time *t* [s]
0	0
1	0.1
1	9.9
0	10

Figure 5.3: Time *t* [s] *vs* Amplitude value A_v [-]

Figure 5.4 shows the whole model structure with all the steps considered in order to develop the simulation. On the first step, 3D geometry, material properties, thermal load calculation and boundary conditions are established as an input. Then, hexahedral volume elements were used for meshing the steel clamping and Cobalt element with an element mesh length l_{mesh} = 2500 µm and l_{mesh} = 200 µm respectfully. The workpiece material was meshed with tetrahedral and hexahedral volume elements. A fine mesh with a mesh width of 25 µm was used for the material areas around the Contact zones to ensure the high quality of simulations results [VITS20, p. 95]. Consequently, the mesh resulted with 156.709 tetrahedral elements and 9.420 hexahedral elements both with quadratic geometry.

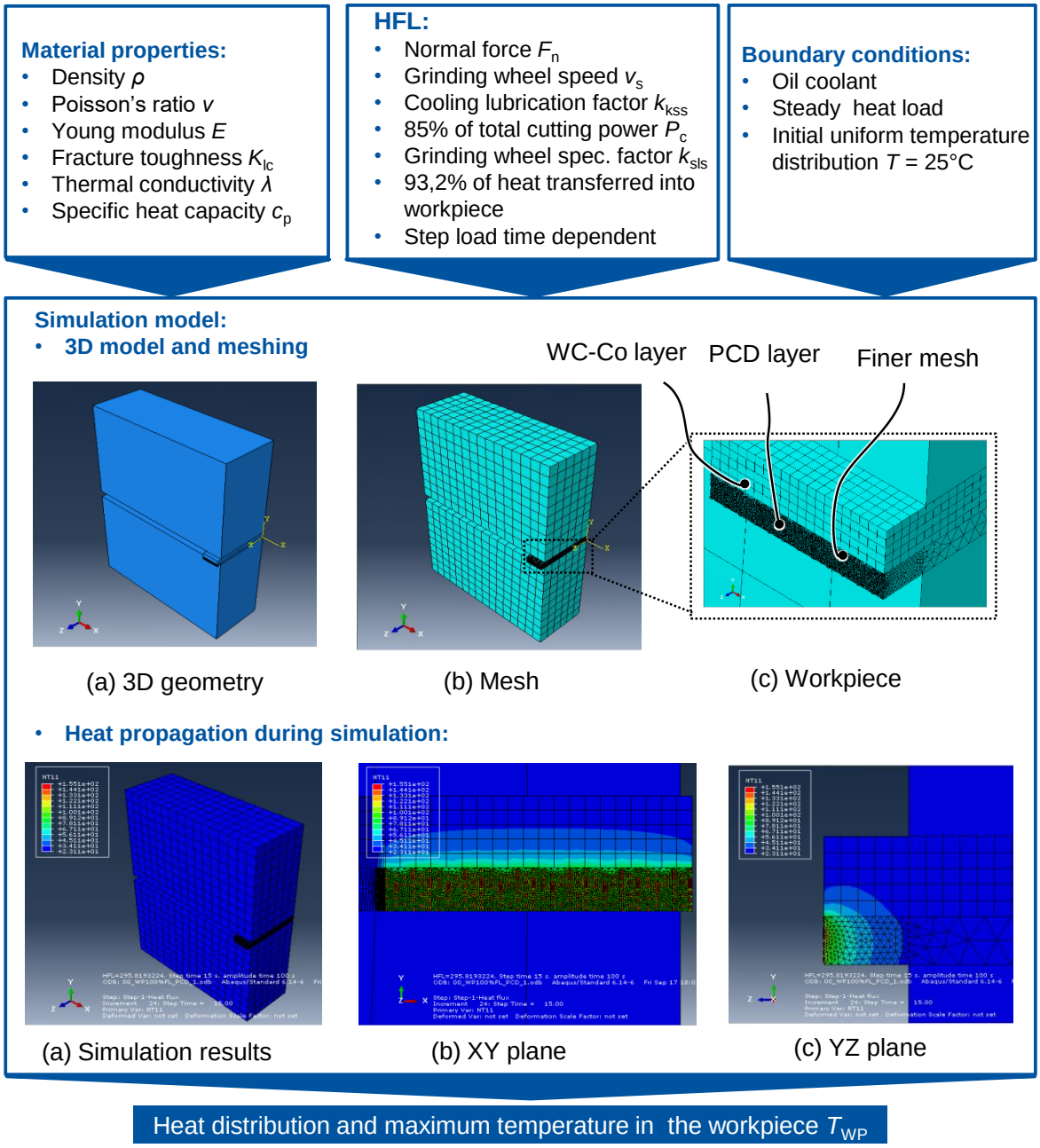

Figure 5.4: FE model for determining the heat distribution and maximum temperature in the workpiece T_{WP}

5.2 Results of the simulation

According to the developed FE model, results of maximum temperature in the workpiece T_{wp} and heat distribution over the workpiece contact zone A_W are discussed among this section. The simulation lasted for t_{sim} = 22 minutes. Then, the heat distribution and maximum temperature in the workpiece T_{wp} are achieved. Figure 5.5 presents these results aforementioned.

As explained in previous sections the grinding power P_c calculated as a function of the grinding and material parameters normal force F_n, grinding wheel speed v_s and fracture toughness K_{Ic} was used as the input variable for the simulation of the workpiece temperatures. Therefore, in the figure 5.5 simulations outcomes for pcBN and PCD are presented.

Although the same simulation model was used for PCD and pcBN specifications, it exists a significant difference in maximum temperature and heat distribution as it is presented. Also, figure 5.5 shows the difficulty to evacuate the heat throughout the length of the workpiece l_w due to low values of thermal conductivity λ for workpieces with less fraction of c-BN $w_{c\text{-}BN}$ such as DCN450 ($w_{c\text{-}BN}$ = 45%) compared with DBW85 ($w_{c\text{-}BN}$ = 85%). Therefore, the less fraction of c-BN $w_{c\text{-}BN}$, the higher maximum temperature in the workpiece T_{WP}.

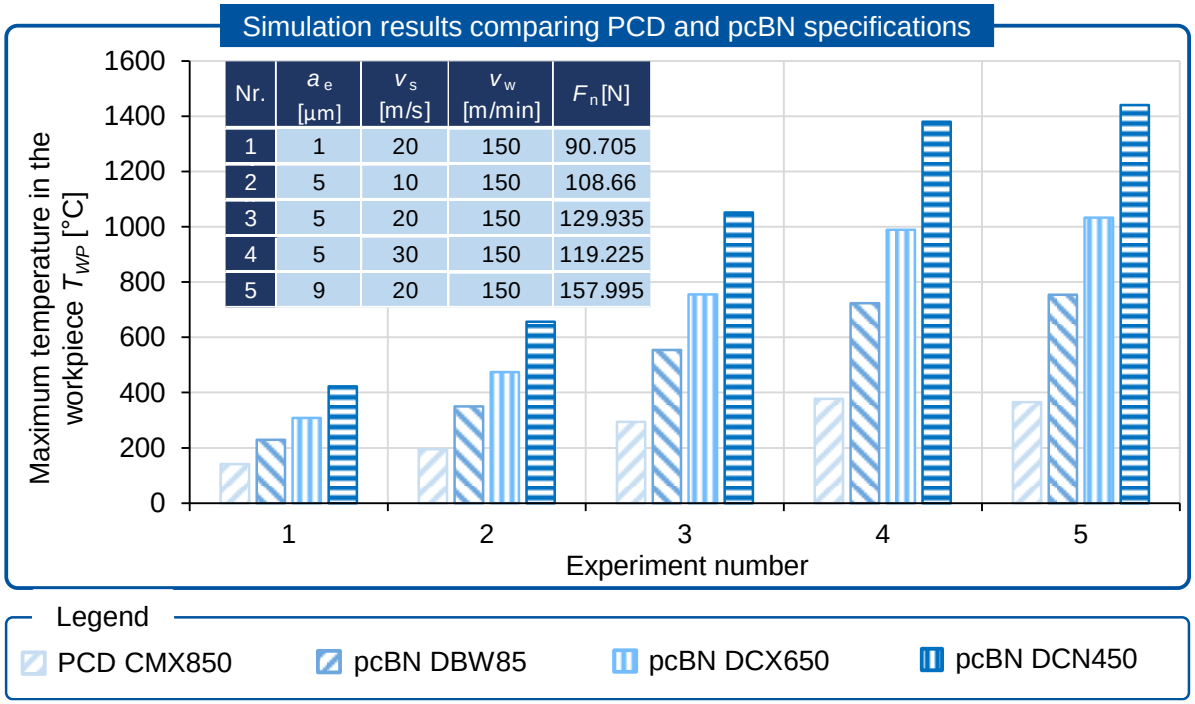

Figure 5.5: Simulation results comparing PCD and pcBN specifications

5.3 Discussion of the results

The lack of experimental data related to this simulation hinders the possibility of demonstrating quantitatively the root cause of these results. Despite of that fact, it is possible to explain the nature of these outcomes based on one reason. The workpiece was assumed as a single part, i.e. there is not a geometrical difference between the grains and the binder. This concept leads to a workpiece model as a single piece with the same properties for the whole composition of binder and grains. Therefore, this fact leads to two possible arguments in regard to this behavior. On one hand, the domination of thermal conductivity λ of grains. On the other hand, the heat accumulation on the contact zone.

5.3.1 Influence of thermal conductivity λ on the maximum temperature in the workpiece T_{WP}

This property is highly influenced by the fraction of grains because of its high value. Theoretical values of thermal conductivity are around $\lambda_{c\text{-}BN}$ = 1300 W/m·K [MORG98, p. 667] or $\lambda_{diamond}$ = 1100 W/m·K [TAY18, p. 1] compared with the ones from the ceramic binder λ_{TiN} = 28.84 W/m·K [MEMS92] or λ_{TiCN} = 25 W/m·K [MATS13, p. 93]. Therefore, this fact leads to a domination of the fraction of grains on the workpiece composition on the thermal conductivity λ of the workpiece.

In the simulation model the thermal conductivity λ is assumed uniform and constant throughout the whole workpiece length l_w with values of λ_{CMX850} = 253.3 W/m·K [VITS20, p. 64] or λ_{DBW85} = 25 W/m·K [MATS13, p. 93] in comparison with values of thermal conductivity λ of grains and binder aforementioned which are heavily different. Therefore, this argument heads to a huge gap compared with real thermal conductivity λ and its resulted maximum temperatures and heat distribution.

Finally, it exists a noticeable difference between thermal conductivity λ of pcBN and PCD correlated to the microstructure. This difference influence directly on thermal conductivity λ. In PCD microstructure diamonds tend to grow, connect and build clusters of grains among each other [YAN18, p. 3]. These structures are able to grow into each other building greater grain structures. Consequently, there are superconductor portions of diamond throughout the workpiece. These structures heavily increase the overall thermal conductivity λ of the whole workpiece. Furthermore, they increase the evacuation of total heat flow q_t introduced. Consequently, the maximum temperature of the workpiece T_{WP} is reduced.

On the other hand, c-BN grains are integrated into ceramic and metallic bonding systems. This bonding systems are naturally isolating materials focused on accumulating heat. Moreover, considering that c-BN does not grow into each other building up greater structure as diamond does, it is reasonable to expect lower thermal conductivity λ and higher maximum temperatures on the workpiece T_{WP} when comparing c-BN and PCD components.

5.3.2 Influence of heat flux load *HFL* on the maximum temperature in the workpiece T_{WP}

Figure 5.6 presents all the maximum temperatures in the workpiece T_{WP} obtained in this simulation where all of pcBN specifications follow a linear trend whereas PCD CMX850 follows a logarithmic trend. According to these results achieved, there exists a linear relationship between the thermal load explained in section 5.1.2 as heat flux load *HFL* and the pcBN specifications. Since the heat flux load *HFL* is a function of normal force F_n, grinding wheel speed v_s and fracture toughness K_{Ic}, a linear relationship is obtained between these parameters and the maximum temperature in the workpiece T_{WP} as well.

On the other hand, the maximum temperature in the workpiece T_{WP} occurs in the same contact zone A_w where it was introduced because. While more heat is introduced in a constant trend as presented in figure 5.3, heat previously introduced is not able to flow. This fact occurs because of the thermal conductivity λ is not high enough to transfer the energy throughout the whole length of the workpiece l_w. Consequently, heat distribution and maximum temperature in the workpiece evolves linearly because it is kept in the same contact zone A_W as it is introduced.

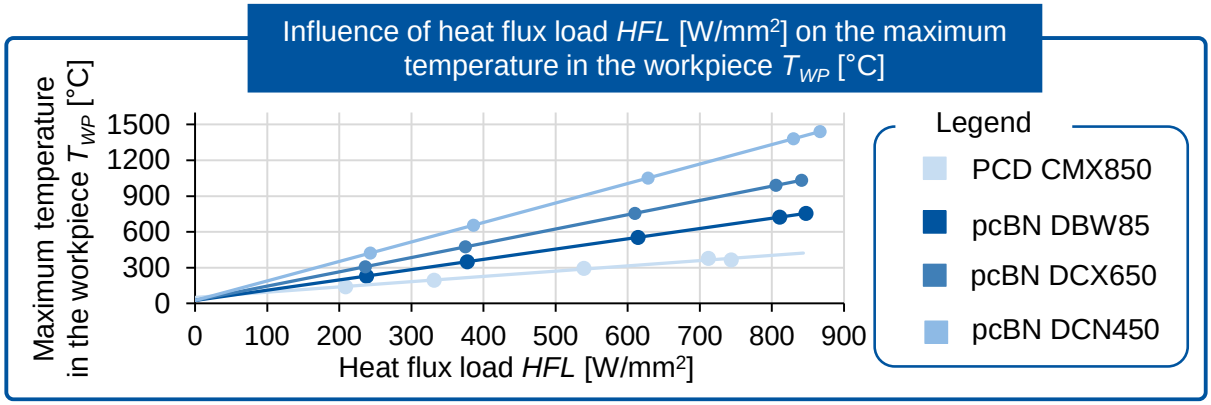

Figure 5.6: Influence of heat flux load *HFL* [W/mm²] on the maximum temperature in the workpiece T_{WP} [°C]

5.4 Intermediate conclusion

In this chapter a finite element model was developed. The aim of this model was to compare the maximum temperature in the workpiece T_{WP} and heat distribution in the contact zone A_W of a PCD CMX850 and different pcBN specification. This thermal load was a function of grinding power P_c based on tribological variables. For this purpose, the model was taken from Vits [VITS20, pp. 79-104]. Material properties and behavior were taken from the literature research showed in table 5.1. The boundary conditions were based on Vits. The thermal load was expressed as heat flux load *HFL.* The heat flux load *HFL* presented in table 5.3 was taken from equation 4.4 based on experiments represented in table 5.2.This load was configured under a step load time dependent as explained in figure 5.3.

The simulation showed a thermal behavior where the maximum temperature in the workpiece T_{WP} and heat distribution resulted in the contact zone A_W of the workpiece. Most of the heat was kept in the workpiece contact zone A_W. In addition, results showed that the lower thermal conductivity λ is, the more the heat accumulated in the contact zone A_W occurs. This fact leads to higher maximum temperature on DCN450 as shown in figure 5.5, because this is the workpiece with less fraction of c-BN $w_{c\text{-}BN}$. Therefore, less thermal conductivity λ.

Since these temperatures are extremely high for a real grinding process for the pcBN specifications, the empirical model proposed in equation 4.5 for PCD is not applicable to pcBN. Consequently, another thermal model with similar material properties, boundary conditions and thermal load should be considered. Nevertheless, these simulations showed a high dependency between the maximum temperature in the workpiece T_{WP} and the heat flux load *HFL*. A minimal modification of this value determined a noticeable change in the result.

In order to decouple the thermal conductivity λ of the simulation model, a more detailed structure of the pcBN workpiece microstructure could be derived in subsequent work. This concept enables the contribution of a more precise determination of the heat transfer mechanism in pcBN grinding. Furthermore, the division of grains and binder into independent structures. Consequently, the influence of thermal conductivity λ on the simulation model could be reduced. As it was showed throughout this chapter, research questions 1 and 2 were answered.

6 Finite element simulation of the thermal load during pcBN grinding

As it was presented in the previous chapter, although the same input parameters of the machine were applied, the resulting maximum temperatures and heat distribution in pcBN and PCD materials were different. On one hand, the thermal properties of the PCBN grains, PCD and binder materials are not the same. On the other hand, considering the grains fraction of volume in the workpiece distribution throughout the workpiece influences the thermal properties and the heat transfer process due to huge difference in values of thermal properties. Therefore, the main objective of this chapter is to mimic as possible the concepts considered by Vits for PCD grinding and complete them with further approaches in order to provide a deeper understanding of the heat transfer process in PCBN workpieces, in this case of DBW85. For that purpose, another model is developed considering further characteristics (section 5.2) with the application different materials and thermal loads (section 5.1). Subsequently, results are discussed in section 5.3.

6.1 Materials and methods

Figure 6.1 presents the research methodology stablished to develop this simulation model. This method is an implementation of the one presented in chapter 5. In particular, this technique provides answers to research questions 3 and 4. For that purpose, this process is divided in four stages as in chapter 5. Phase I was presented in section 5.1.1 from previous chapter. Also, the explanation was completed in section 6.1.1. Subsequently, subsections from 6.1.2 to 6.1.3 explain phases II and III. All the specifications about the geometrical and simulation model are presented. Finally, results achieved are shown in section 6.2 and then discussed in section 6.3.

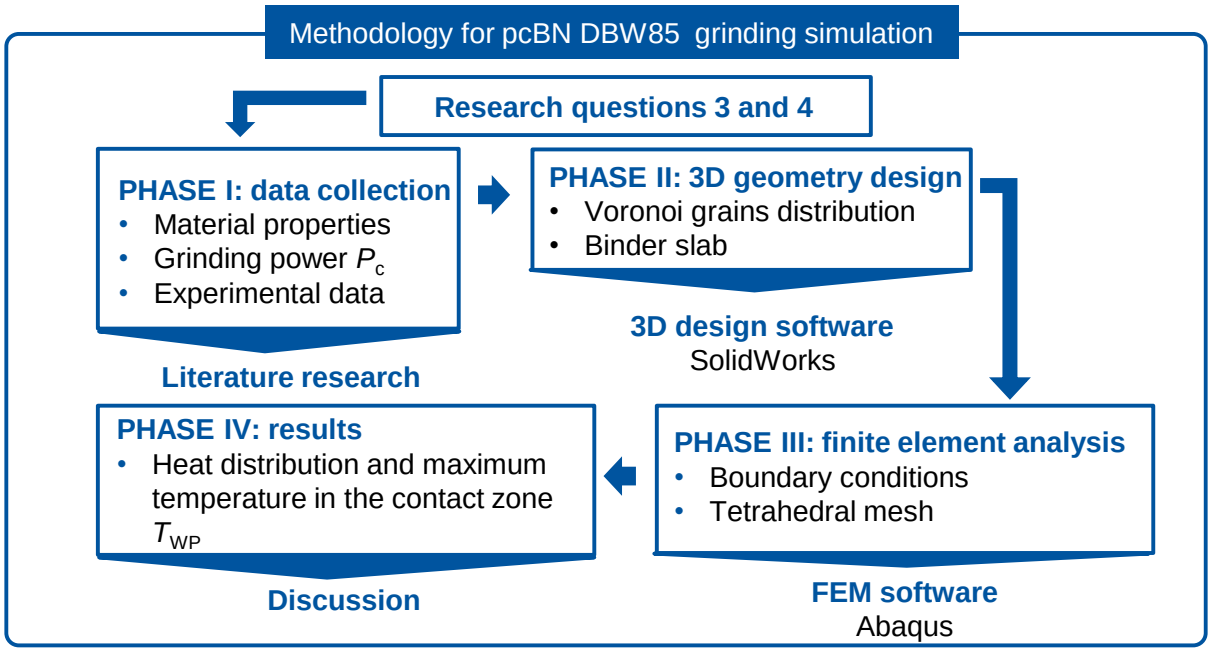

Figure 6.1: Research methodology for simulation of single grain temperature during pcBN DBW85 grinding

6.1.1 Determination of material properties and thermal load

As it was mentioned in section 5.1.1, in this model material are considered temperature-dependent, isotropic and elastic material behavior without chip formation. According to these behaviors, material properties of c-BN grains and AlWCoB binder applied into the model are mentioned in table 5.1. In addition, in this case fracture toughness K_{Ic} was not considered because the thermal model applied to calculate the heat flux load *HFL* did not take it into account.

It has been demonstrated according to results earlier mentioned in chapter 5 that the mathematical model proposed by Vits is only useful for PCD materials. Accordingly, there is not any possibility of obtaining a reasonable heat flux load *HFL* as input for the simulation model. Therefore, it exists a lack of a mathematical model that provides the thermal load from grinding power P_c during grinding pcBN. Consequently, experimental data of pcBN DBW85 was chosen in order to apply a reasonable thermal load. The maximum temperature in the DBW85 workpiece T_{DBW85} was measured by Kaiser.

Table 6.1 presents the experimental data applied in this simulation. These experiments were focused on varying the normal force F_n, but fixing the grinding wheel speed v_s. Three different pcBN specifications were investigated in the experiment. Only pcBN DBW85 was applied for the simulation. According to these experiments where the maximum temperature in the DBW85 workpiece T_{DBW85} was measured. The influence of the specific normal force F_n, the grinding wheel speed v_s and the PCBN specification on the coefficient of friction μ.

Table 6.1: Experimental data description [KAIS20, p. 51]

Experiment number	Grinding wheel speed v_s [m/s]	Specific normal force F_n'' [N/mm²]	Specific grinding power P_c'' [W/mm²]	Grinding power P_c [W]
1	10	6.3	22.12	210.58
2	10	8.4	22	209.44
3	10	10.5	34.03	323.96

6.1.2 Structure of simulation model

This simulation model was built on the same assumptions as explained in sections 5.1.2 and 5.1.3. Nevertheless, in this case the 3D geometry was modified in order to get a different approach in regard to the heat transfer mechanism through the workpiece. For that purpose, grains and binder were sketched as different models and then joined together with the proper volume dimensions with the aim of reaching fraction volume of grains $w_{c\text{-}BN}$ = 85%. This first model of the c-BN grains was modeled according to a Voronoid tessellation. Then, the model of the binder AlWCoB was modeled as a slab taken into consideration the volume of grains. Once the geometrical model was completed, boundary conditions, steps, heat flux load *HFL* and step load time dependent were applied following the same method as it was explained in chapter 5.

Voronoi Tessellation

One of the main objectives of this part of the simulation was to develop a model where the grains are distributed randomly throughout the length of the workpiece. For that purpose, spatial tessellation is a reasonable approach to design the 2D irregular geometry of polycrystal structures. Figure 6.2 shows a Voronoi tessellation which are a practical application for material structure modeling [BURT15, p. 2].

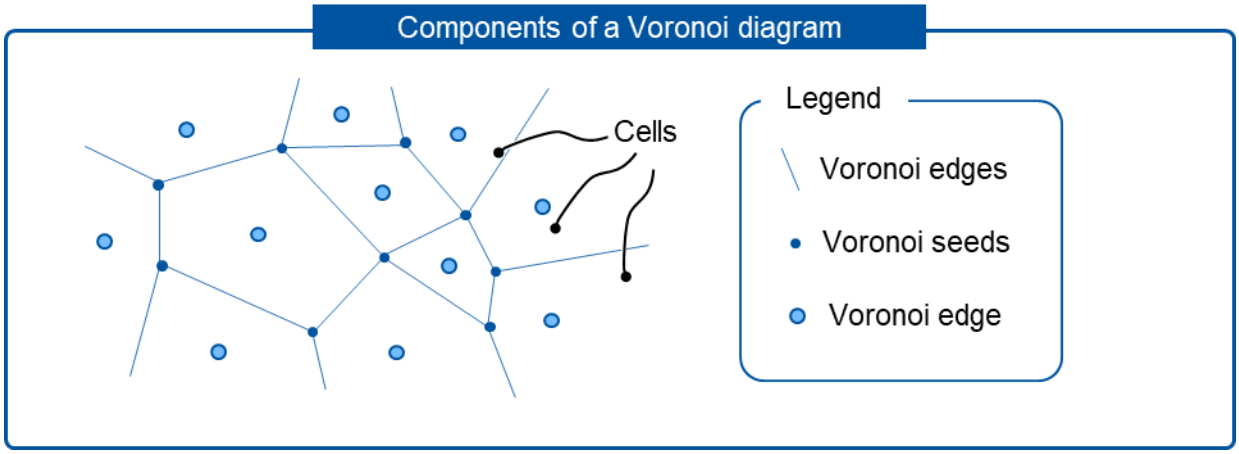

Figure 6.2: Components of a Voronoi diagram [BURT15, p. 3]

Given a finite set of distinct, isolated points in a continuous space, defined as seeds, we associate all locations in that space with the closest member of the point set. The result is a partitioning of the space into a set of regions, also defined as cells. This set of cells is referred as Voronoid diagram [OKAB00, p. 1]. This pattern which can be found in nature such as skin of a giraffe or soap bubbles, is applied in several disciplines such as computational geometry, biology or physics, but more interest is laid on modelling physical-chemical systems [OKAB00, p. 468]. Furthermore, Aparicio et al. demonstrated that the distribution of volume of Voronoi polyhedral is a natural representation of a random array of spheres that seems to be particularly useful for studying the sintering of fine particles as it is the case of the workpiece to be modelled [APAR95, p.]. For that purpose, a C++ program obtained from the literature was used with the aim of creating the Voronoi diagram.

This software was designed using the program Qt creator from TrollTech. In this program parameters horizontal h_{Qt} as number of grains in horizontal direction. Vertical v_{Qt} as number of grains in vertical direction. Spacing s_{Qt} as distance between grains. Disturbance d_{Qt} as curvature of edges of the grains. Then, offset o_{Qt} as distance between frame that surrounds the grains distribution and grains allow to design the specific Voronoi tessellation as it is shown in figure 6.3.a and 6.3.b In addition, the units of these parameters were not specified. Consequently, final dimensions were only known when the DXL file was opened [GITH18]. Figure 6.3.c is shown the DXF file with the desired parameters which in this case were h_{Qt} = 3 grains, vertical v_{Qt} = 3 grains, spacing s_{Qt} = 50, d_{Qt} = 0 % and offset o_{Qt} = 0.

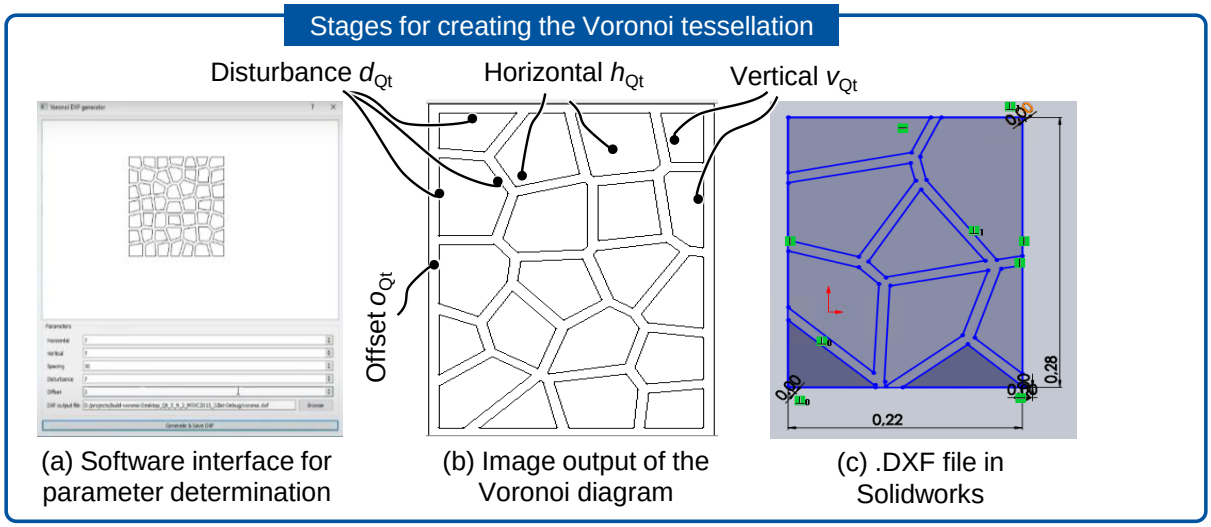

Figure 6.3: Stages for creating the Voronoi tessellation

3D geometry for cubic boron nitride grains and AlWCoB binder

Once the Voronoi diagram was transferred into a DXL file, the sketch was opened in the software Solidworks. The procedure followed to develop the grain volume model is explained as following. Figure 6.4.a shows the height of the tetrahedron h_t = 5 cm was stablished according to the grain diameter d_g = 1-2 µm provided in the literature [MULL21, p. 1150]. The reason because this amount was chosen is based on scaling down the volume later. Furthermore, the software was not working properly when dimensions in microns were introduced.

Same procedure was followed for every grain in the complete distribution due to the geometry of the initial sketch. This geometry that the Voronoi diagram which the software returns is not a closed area, i.e. the cell mentioned in the previous section are not close. Therefore, it is necessary to develop the closed area that constructs the base for the pyramid. This pyramid will build the whole tetrahedron as it is shown in figure 6.4.b.

Stages for creating the Voronoi tessellation

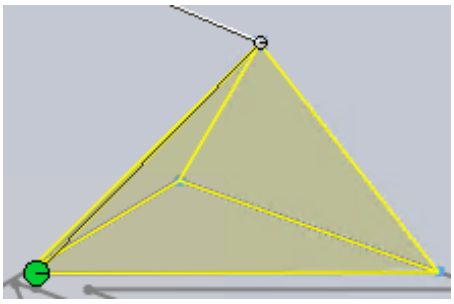

(a) 3D geometry of a single crystal

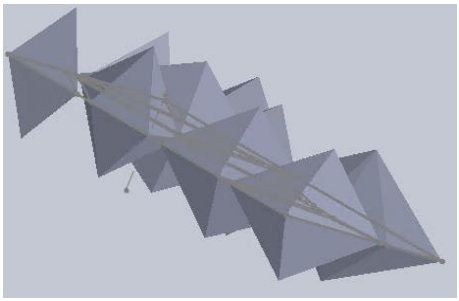

(b) Grain distribution according to Voronoi tessellation

Figure 6.4: 3D geometry for Voronoi grain distribution

On the other hand, the slab is made by extruding the area that surrounds the sketch. This plane was initially used in the Voronoi diagram explained in the previous section. In particular, this procedure was done by following the objective of reaching the fraction of grain volume $w_{c\text{-}BN}$ = 85%. For that purpose, once the slab and the Voronoi grain distribution were built, the height of the extrusion was modified, and the volume of grains was scaled down by an iterative method. This activity was done until a fraction of grains volume $w_{c\text{-}BN}$ = 86,53% was reached. Therefore, figure 6.5 and table 6.2 present the dimensions of both parts. Although the fraction of grain volume w was reached, the final geometry of the workpiece as it was used in the experiments done by Kaiser were not obtained.

Components of the simulation model

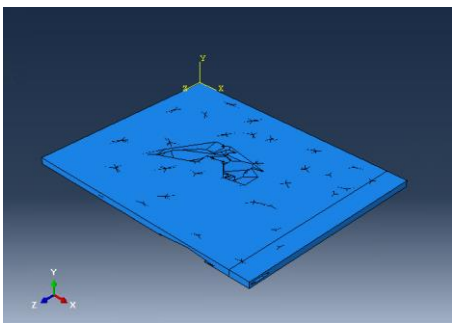

(a) Empty slab

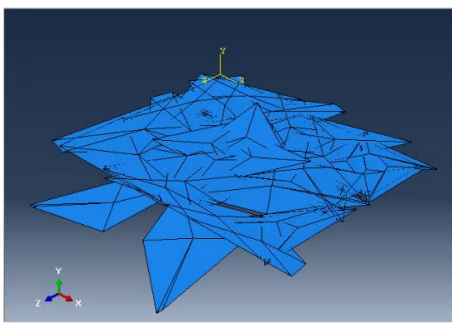

(b) Voronoi grain distribution

Figure 6.5: Components of the simulation model

Table 6.2: Dimensions of the components from the simulation model

Dimension	Unit	Slab	Voronoi grain distribution
Width	mm	220	-
Height	mm	7.11	-
Length	mm	280	-
Volume	mm^3	49628.62[1]	318888.52

[1] This value is the result of removing the volume of the Voronoi grain distribution from the whole slab.

6.1.3 Steps for the simulation model

Figure 6.6 summarizes all the inputs taking from the previous model which were discussed in detail in chapter 5. Moreover, all the geometrical properties relative to the grains and binder were modified as defined in sections aforementioned. Also, results obtained on experiments done by Kaiser were applied on this workpiece model.

Tetrahedral volume elements were used for meshing both parts. On one hand, the slab was divided in two parts in which different mesh can be found following the same procedure as previous model. One part with a finer mesh where the heat input was applied. This mesh had an element mesh length l_{mesh} = 3000 µm. A thicker mesh was applied to the rest of the part with an element mesh length l_{mesh} = 13000 µm. This assumption was applied because no heat was reaching that portion of volume, as demonstrated in figure 6.6. As a result of this mesh, a total of 13721 elements were obtained. On the other hand, the Voronoi grain distribution was meshed up with an element mesh length l_{mesh} = 10000 µm. Consequently, 22703 elements were found throughout this part. No partition was made due to the high complex geometry in this part. Finally, the model reached a total of 36424 tetrahedral elements with quadratic geometry as it is shown in the figure 6.6. The selection of these parameters was based on lowering simulation time t_{sim}.

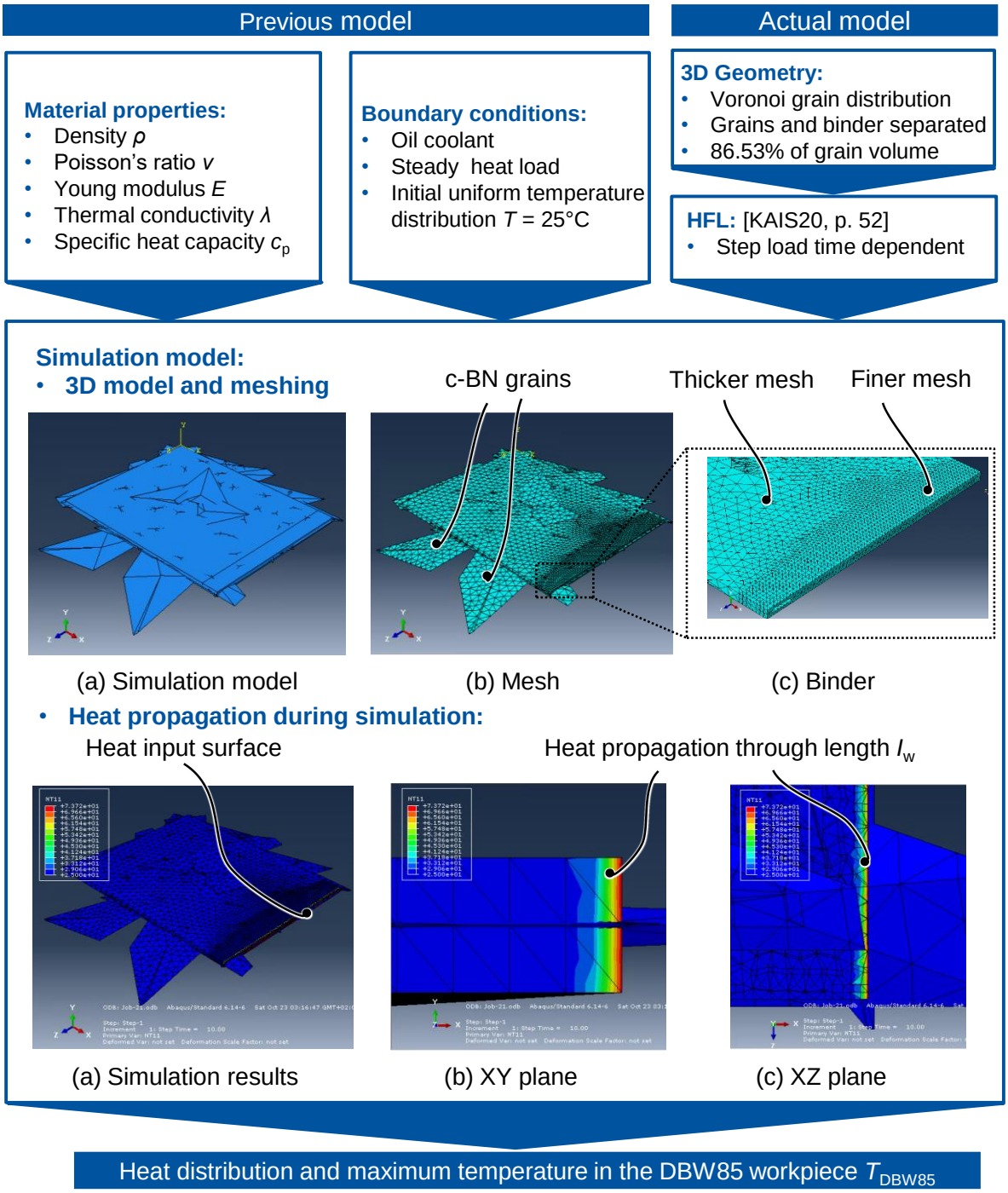

Figure 6.6: FE model for determining the heat distribution and maximum temperature in the DBW85 workpiece

6.2 Results of the simulation and discussion

The results of heat distribution and maximum temperature in the DBW85 workpiece T_{DBW85} on contact zone A_W for this second simulation model are presented and discussed throughout this section. After running the simulation, the heat distribution and maximum temperature in the DBW85 workpiece T_{DBW85} thanks to the grinding power P_c calculated as a function of the grinding parameters from Kaiser. These parameters were normal force F_n, grinding wheel speed v_s and friction coefficient μ_s. Also, grinding power P_c was applied as the heat input for the simulation of the DBW85 workpiece temperatures. As a result of the

simulation of all these variables applied in the aforementioned model, figure 6.7 presents a comparison between simulated and measured temperature values.

6.2.1 Influence of cutting power P_C [W] on maximum temperature in the DBW85 workpiece T_{DBW85} [°C]

Figure 6.7 shows the difference between measured and simulated results are noticeable. The reasons for these values are based on 3 facts. On one hand, the measured values are not exactly precise due to the complexity of measurement of the exact temperature of the grain T_{grain}. On the other hand, the simulation does not embrace all the conditions that the experiment represent. In particular, the workpiece modeled does not strictly follow the geometry that it was used in the experiments. Finally, as commented in section 6.1.1, during these simulations it was assumed that all the grinding power P_c was converted into heat. This fact was based on the lack of an empirical-analytical model that allows to divide the mechanical and thermal load. Consequently, it was assumed that all the power was converted into heat although this assumption does not represent the real process. Considering the mechanical load is a noticeable assumption to take into account.

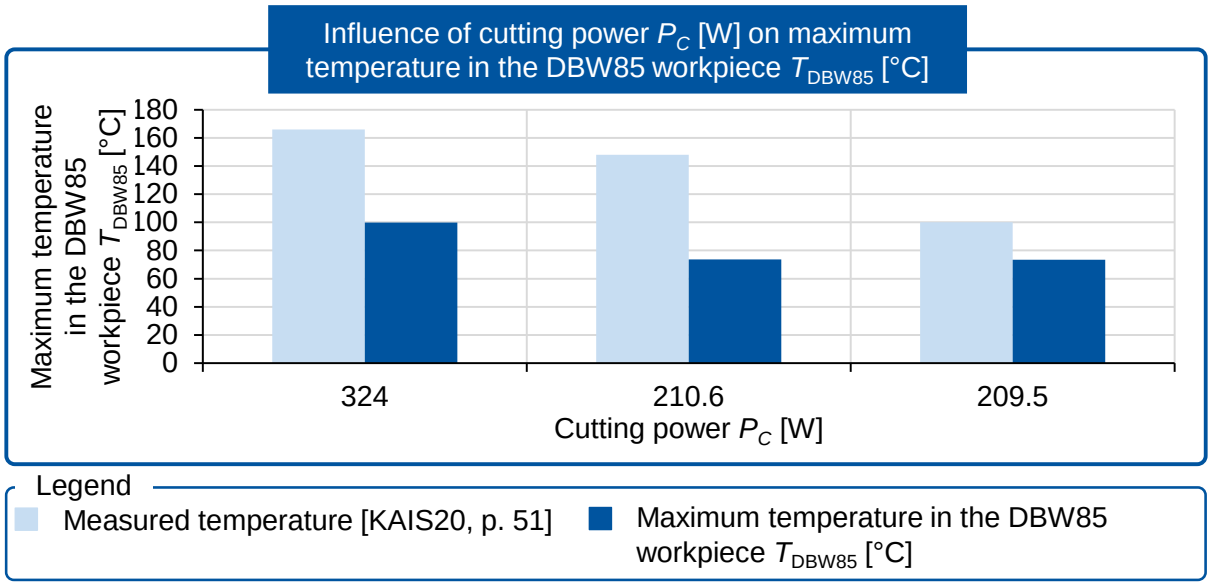

Figure 6.7: Influence of cutting power P_C [W] on maximum temperature in the DBW85 workpiece $T_{WP\ DBW85}$ [°C]

Figure 6.8 shows a linear trend of both measured and simulated data. These results follow similar path. This fact is due to the direct proportional relationship between grinding power P_c and maximum temperature in the DBW85 workpiece T_{DBW85}. Although no analytical formula was provided to proof the correlation between these two variables and the existence of significant lack of experimental data, it is reasonable to assume a priori a linear evolution of the maximum temperature in the DBW85 workpiece T_{DBW85} on the grinding power P_c as it is presented in this figure.

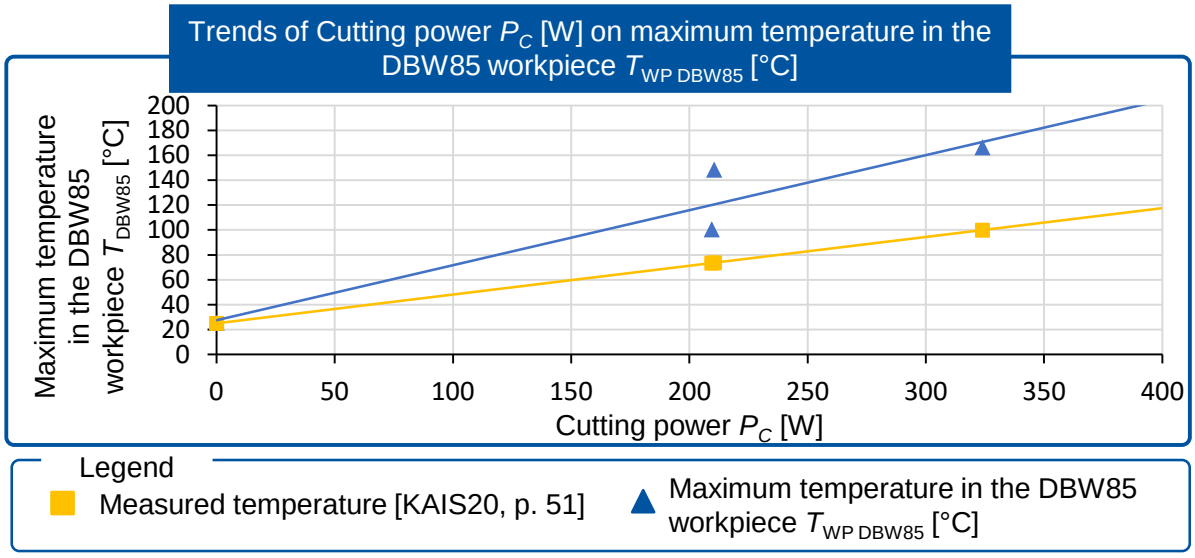

Figure 6.8: Trends of Cutting power P_C [W] on Maximum temperature in the DBW85 workpiece T_{DBW85} [°C]

In this model the thermal conductivity λ of the whole workpiece was modified in order to modify the heat distribution. Nevertheless, figure 6.6 presents a significantly similar thermal behavior as it occurred in model form chapter 5. In this case, the heat distribution is kept in the contact zone A_W and maximum temperature in the DBW85 workpiece T_{DBW85} are achieved in that area as well. In addition to previous reasoning, the heat distribution through the XZ plane does not move forward through the length of the DBW85 workpiece and it is kept in the binder. In contrast, it is noticeable that there exists a difference in temperature between pcBN grain and binder components. Therefore, modelling the part in this manner supposes a reasonable hypothesis, because models simulated keep the temperature in the similar volume portion.

6.3 Intermediate conclusion

Similarly as it was done in chapter 5, another finite element model was developed. The aim of this model was to predict the maximum temperature in the DBW85 workpiece T_{DBW85} and heat distribution in the contact zone A_W. The thermal load was determined by the grinding power P_c based on tribological variables. For this purpose, a model was built where the 3D geometry was divided into 2 separated parts as showed in figure 6.5. The grains were modeled according to a Voronoi tessellation, and the binder modeled as a slab. This slab was made by removing the volume of grains from its inside. This measure was made with the objective of obtaining a fraction of grains volume $w_{c\text{-}BN}$ = 85% were a $w_{c\text{-}BN}$ = 86,53% was finally reached. After meshing all the geometry, 36.424 tetrahedral elements with quadratic geometry were obtained.

Model inputs were acquired from different sources. Material properties of pcBN DBW85 were taken from the literature. This data is showed in table 5.1. The boundary conditions were followed as stablished in chapter 5 and the thermal load was taken from experiments of Kaiser [KAIS20, p. 52]. These experimental results are shown in table 6.1. This load was expressed as heat flux load *HFL.* It was configured under a step load time dependent as explained in figure 5.3.

The simulation presented a similar thermal behavior where the maximum temperature in the DBW85 workpiece T_{DBW85} and heat distribution resulted in the contact zone A_W. All this heat was kept in the surface as it occurred in chapter 5 with all other pcBN specifications. Also, it

was proven that values simulated and measured for this workpiece follow similar linear trends. Moreover, values obtained had similar order of magnitude.

In contrast, no validation was carried out since the simulation did not replicate exactly the experiment conditions. Also, the fact that the high measurement uncertainty while measuring single grain temperature difficult the experiment modeling.

A further look could be taken into a better modeling of the workpiece by respecting the Voronoi distribution, geometry and fraction of grain volume *w*. Also, distributing the grains more homogeneously through the binder slab in different planes instead of all the grains concentrated in one plane. This fact could increase the heat flow q_t through the workpiece length l_w. Moreover, different polyhedron geometry could be applied. Some other examples to model the grains in a different manner could be hexahedron or dodecahedron. Therefore, as it was showed throughout this chapter, research questions 3 and 4 were answered.

7 Summary and outlook

7.1 Summary of the findings

The graphitization of diamond, the low hardness H_v of graphite and the difficulty to measure single grain temperature while grinding are significant problems to overcome. These facts could lead to an increase of efficiency and costs reduction of grinding process. For that purpose, simulations were conducted based on a finite element model. This model makes possible to predict the heat distribution and maximum temperature in the workpiece T_{WP} during PCD and pcBN grinding. Consequently, it was stated that the research objective was to develop a model that simulates the temperature of single grains during surface grinding in the workpiece contact zone A_W for different pcBN specifications.

In regard to reach that purpose, research question 1: “How can the empirical-analytical model made from PCD be applied to pcBN?” and research question 2: “How much differs the heat transfer mechanism between PCD and pcBN?” were answered in chapter 5. For that purpose, a comparison of the heat distribution and maximum temperature in the workpiece T_{WP} in the contact zone A_W between PCD CMX850 workpiece and different pcBN specification was stablished. These results were functions of the grinding power P_c based on tribological variables and material properties.

Simulation results were high up to T_{WP} = 1441°C compared with the ones from PCD CMX850. Therefore, the empirical-analytical model proposed from Vits for PCD is not applicable for pcBN. So, another thermal model with similar material properties, boundary conditions and thermal load should be considered.

In chapter 6 research question 3: “How much does the workpiece microstructure affect the heat distribution and maximum temperature?” was investigated. For that purpose, a similar model as done in chapter 5 was applied. In this case, binder and grains were modeled in separated parts. Moreover, the grains followed a Voronoi distribution. Then, the results showed similar behavior as aforementioned models. Nevertheless, both measured and simulated data from pcBN DBW85 followed similar trends and order of magnitude. In contrast, no validation was carried out with these results since the simulation did not replicate exactly the experiment conditions.

Finally, research question 4: “How can temperatures and heat distribution during grinding of different pcBN specifications be predicted with a FE model?” was answered in both chapters 5 and 6. Although similar results were obtained in chapter 6 and it was proven that this model followed a linear trend, there existed a significant gap between measured and simulated temperature. On the other hand, the model used in chapter 5 showed that PCD and pcBN specifications followed different trends regarding simulated temperature. In this case, all the pcBN specifications followed same linear trend. Therefore, numerical values differed sufficiently to answer question 4 in such a way that improvement needs to be done in simulation models. Nevertheless, it was proven that it exists a higher dependency of the model from the thermal load defined as heat flux load *HFL* rather than the 3D geometry of the model.

In conclusion, the research objective was to develop a model that simulates the temperature of single grains during surface grinding in the workpiece contact zone A_W for different pcBN specifications was partially achieved although not all results paired with the measured ones.

7.2 Outlook for further investigations

First of all, further investigations on the field of thermal load should be done. In particular, finding out the fraction of heat introduced from the total grinding power P_C. Also, reaching an

empirical-analytical model that provides a precise heat flux load *HFL* is a significant topic. This mathematical formulation could help in developing more accurate simulations. This model could be achieved by using experimental data from Kaiser. The motivation of following this path is based on the high influence on the thermal load on the simulation model as it was proven in sections 5.3 and 6.2. Therefore, the more precise the empirical-analytical model is, the closer the simulated results should be related to the measured ones.

Once there is a solid mathematical model, improving the 3D geometry of the model could provide a better outlook to understand the heat transfer mechanism on grains. By using the Voronoi diagram applied in several sketches, numerous layers of grains can be achieved. This fact enables the possibility of reaching the proper fraction of grains volume *w*. Consequently, several pcBN specifications can be applied. Then, applying similar boundary conditions and material properties from the literature could provide robust characteristics for the simulation model.

If previous assumptions related to the empirical-analytical model and 3D geometry of the surface do not provide any acceptable result. Then, changing the simulation software could be a good opportunity to finally understand the heat transfer mechanism throughout the binder and grains. Some possibilities to choose from were presented in section 2.4. Therefore, looking at results from chapter 5 and 6, the following research hypothesis can be formulated for a future research work:

The simulation of the pcBN workpiece enables the construction of a finite element model that can simulate the single grain temperature through the workpiece in pcBN grinding with grains modeled using a Voronoi tessellation and a thermal load model as a function of normal force F_n, grinding wheel speed v_s and fracture toughness K_{Ic}.

V Bibliography

[AGME18] Agmell, M.; Bushlya, V.; Laakso, S. V. A. et al.: Development of a simulation model to study tool loads in pcBN when machining AISI 316L. In: International Journal of Advanced Manufacturing Technology, Vol. 96, 2018, pp. 2853–2865.

[ALCA16] Alcantar-Peña, J. J.; Montes, J.; Arellano-Jimenez, M. J. et al.: Low temperature hot filament chemical vapor deposition of Ultrananocrystalline Diamond films with tunable sheet resistance for electronic power devices. In: Diamond and Related Materials, Vol. 69, 2016, pp. 207–213.

[ANDE90] Anderson, J. C.; Leaver, K.D.; Alexander, J.M.: Material science. 4th edition. Springer-Science +Business Media, Singapore, 1990.

[APAR95] Aparicio, N. D.; Cocks, A. C. F.: On the representation of random packing spheres for sintering simulations. In: Acta Metallurgica et Materialia, Vol. 43, 1995, pp. 3873–3884.

[ARSE05] Arsecularatne, J. A.; Zhang, L. C.; Montross, C.: Wear and tool life of tungsten carbide, PCBN and PCD cutting tools. In: International Journal of Machine Tools and Manufacture, Vol. 46, 2005, pp. 482–491.

[BENK99] Benko, E.; Stanisław, J. S.; Królicka, B. et al.: cBN–TiN, cBN–TiC composites: chemical equilibria, microstructure and hardness mechanical investigations. In: Diamond and Related Materials, Vol. 8, 1999, pp. 1838–1846.

[BREV04] Breviary Technical Ceramics: Tribological systems, 2004. URL: http://www.keramverband.de/brevier_engl/5/7/1/5_7_1_2.htm.

[BRIN06] Brinksmeier, E.; Aurich, J. C.; Govekar, E. et al.: Advances in Modeling and Simulation of Grinding Processes. In: CIRP Annals, Vol. 55, 2006, pp. 667–696.

[BUND55] Bundy, F. P.; Hall, H.T.; Strong, H.M. et al.: Man-made diamonds. In: Nature, Vol. 176, 1955, pp. 51–55.

[BUND62] Bundy, F. P.; Wentorf, R. H.: Direct Transformation of Hexagonal Boron Nitride to Denser Forms. In: Journal of Chemical Physics, Vol. 38, 1962, pp. 1144–1149.

[BUND67] Property right CA 754992-A (21.03.1967). Bundy, F. P.: Method of producing cubic boron nitride.

[BUND89] Bundy, F. P.: Pressure-temperature phase diagram of elemental carbon. In: Physica A: Statistical Mechanics and its Applications, Vol. 156, 1989, pp. 169–178.

[CAGG14] Caggiano, A.: Fuzzy Logic. In: L. Laperrière, G. Reinhart (Eds.): CIRP Encyclopedia of Production Engineering. Berlin, Springer, pp. 562–568.

[CHEN20] Chen, Z.; Ma, D.; Wang, S. et al.: Wear resistance and thermal stability enhancement of PDC sintered with Ti-coated diamond and cBN. In:

International Journal of Refractory Metals and Hard Materials, Vol. 92, 2020, pp. 1–9.

[CHEN09] Cheng, K.: Machining Dynamics. Springer, London, 2009.

[CHIL00] Childs, T.; Maekawa, K.; Obikawa, T. et al.: Metal Machining - Theory and Applications. Arnold, London, 2000.

[CHO18] Cho, W. J.; Shon, I. J.: Effect of BN Addition on the Mechanical Properties of TiN-BN Composites. In: Korean Journal of Metals and Materials, Vol. 56, 2018, pp. 658–663.

[CORR75] Corrigan, F. R.; Bundy, F. P.: Direct transitions among the allotropic forms of boron nitride at high pressures and temperatures. In: Journal of Chemical Physics, Vol. 63, 1975, pp. 3812–3820.

[DADD14] D'Addona, D.M.: Artificial Neural Netwotk. In: L. Laperrière, G. Reinhart (Eds.): CIRP Encyclopedia of Production Engineering. Berlin, Springer, pp. 911–919.

[DAVI74] Davidson, A. (Ed.): Handbook of precision engineering. Production engineering, 11, Phillips, Eindhoven, 1974.

[DAVI09] Davim, J. P.; Jackson, M. J. (Eds.): Nano and micromachining. John Wiley & Sons, New Jersey, 2009.

[DIN79] DIN 50320 (December 1979). Wear; Terms, Systematic Analysis of Wear Processes, Classification of Wear Phenomena.

[DIN20] DIN 8580 (January 2020). Manufacturing processes - Terms and definitions, division.

[DIN88] DIN 50323 (November 1988). Tribology; terms.

[DIN03] DIN 8589-11 (September 2003). Manufacturing processes chip removal - part 11 Grinding with rotating tool.

[DING05] Ding, X.; Liew, W.Y.H.; Liu, X. D.: Evaluation of machining performance of MMC with PCBN and PCD tools. In: 15th International conference on wear of materials, Vol. 259, 2005, pp. 1225–1234.

[DOBR13] Dobrinets, I. A.; Vins, V. G.; Zaitsev, A. M.: HPHT-Treated Diamonds. Springer, Berlin, 2013.

[DUCO19] Ducobu, F.; Rivière-Lorphèvre, E.; Galindo-Fernandez, M. et al.: Coupled Eulerian-Lagrangian (CEL) simulation for modelling of chip formation in AA2024-T3. In: Procedia CIRP, Vol. 82, 2019, pp. 142–147.

[ECKE71] Structure Data of Elements and Intermetallic Phases AgB-FePB, 1971. URL: https://materials.springer.com/lb/docs/sm_lbs_978-3-540-36859-5_7.

[EYHU05] Eyhusen, S.: Phase formation processes in the synthesis of boron nitride films. Dissertation, University of Göttingen, 2005.

[EN05] EN 843-4 (June 2005). Advanced technical ceramics – Mechanical properties of monolithic ceramics at room temperature - Part 4: Vickers, Knoop and Rockwell superficial hardness.

[FUJI09] Fujisaki, K.; Yokota, H.; Furushiro, N. et al.: Development of ultra-fine grain binderless cBN tool for precision cutting of ferrous materials. In: Journal of Materials Processing Technology, Vol. 209, 2009, pp. 5646–5652.

[GITH18] GitHub: Voronoi, 2018. URL: https://github.com/bonafid3/Voronoi.

[GUO00] Guo, C.; Malkin, S.: Energy Partition and Cooling During Grinding. In: Journal of Manufacturing Processes, Vol. 2, 2000, pp. 151–157.

[GUO99] Guo, C.; Wu, Y.; Varghese, V.; Malkin, S.: Temperatures and Energy Partition for Grinding with Vitrified CBN Wheels. In: CIRP Annals, Vol. 48, 1999, pp. 247–250.

[ISO12] ISO 513 (November 2012).Classification and application of hard cutting materials for metal removal with defined cutting edges - Designation of the main groups and groups of application.

[IRIF03] Irifune, T.; Kurio, A.; Sakamoto, S.; Sumiya, H.: Ultrahard polycrystalline diamond from graphite. In: Nature, Vol. 421, 2003, pp. 599–600.

[JACK91] Jackson, A.G.: Handbook of Crystallography : For Electron Microscopists and Others. Springer, Michigan, 1991.

[JIAN03] Jiang, X.; Philip, J.; Zhang, W. J. et al.: Hardness and Young's modulus of high-quality cubic boron nitride films grown by chemical vapor deposition. In: Journal of Applied Physics, Vol. 93, 2003, pp. 1515–1519.

[KAIS20] Kaiser, J.: Tribologie beim Schleifen von PCBN mit Diamantschleifscheiben. Bachelor thesis, RWTH Aachen, 2020.

[KAKA04] Kakani, S. L.; Kakani, A.: Material science. New Age International, New Delhi, 2004.

[KANY16] Kanyanta, V. (Ed.): Microstructure-Property Correlations for Hard, Superhard, and Ultrahard Materials. Springer, Cham, 2016.

[KAPO17] Kapoor, R.: Severe Plastic Deformation of Materials. In: A.K. Tyagi, S. Banerjee (Eds.): Materials Under Extreme Conditions: Recent Trends and Future Prospects. Netherlands, Elsevier, pp. 717–754.

[KASO16] Kasonde, M.; Kanyanta, V.: Future of Superhard Material Design, Processing and Manufacturing. In: V. Kanyanta (Ed.): Microstructure-Property Correlations for Hard, Superhard, and Ultrahard Materials. Cham, Springer, pp. 221–239.

[KLOC09] Klocke, F.: Manufacturing Processes 2 - Grinding, Honing, Lapping. Springer, Berlin, 2009.

[KLOC11] Klocke, F.: Manufacturing Processes 1 - Cutting. Springer, Berlin, 2011.

[KLOC14] Klocke, F.: chip formation. In: L. Laperrière, G. Reinhart (Eds.): CIRP Encyclopedia of Production Engineering. Berlin, Springer, pp. 178–179.

[KRAU74] Kraus, J.: Tribology. In: A. Davidson (Ed.): Handbook of precision engineering. Production engineering, 11. Eindhoven, Phillips, pp. 121–183.

[LAPE14] Laperrière, L.; Reinhart, G. (Eds.): CIRP Encyclopedia of Production Engineering. Springer, Berlin, 2014.

[LI20] Li, Ming-Liang; Liang, Li-Xing; Wang, Hai-Long et al.: Processing and properties of PcBN composites fabricated by HPHT using PSN and Al as sintering additive. In: Journal of rare metals, Vol. 39, 2020, pp. 570–576.

[LI18] Li, J.; Meng, W.; Dong, K. et al.: Study of Effect of Impacting Direction on Abrasive Nanometric Cutting Process with Molecular Dynamics. In: Nanoscale research letters, Vol. 13, 2018, pp. 11.

[LIU14] Liu, G. D.; Kou, Z. L.; Yan, X. Z. et al.: Sintering of Fine-Grained Polycrystalline Cubic Boron Nitride Compacts without Binder. In: Applied Mechanics and Materials, Vol. 665, 2014, pp. 79–84.

[LOOS15] Loos, M. (Ed.): Carbon Nanotube Reinforced Composites. Elsevier, Berlin, 2015.

[LOOS15] Loos, M.: Allotropes of Carbon and Carbon Nanotubes. In: M. Loos (Ed.): Carbon Nanotube Reinforced Composites. Berlin, Elsevier, pp. 73–101.

[LUDE19] Ludema, K. C.; Ajayi, L.: Friction, Wear, Lubrication. Chapman and Hall, Milton, 2019.

[LYU16] Lyu, Y.; Bergseth, E.; Olofsson, U.: Open System Tribology and Influence of Weather Condition. In: Scientific reports, Vol. 6, 2016, pp. 32455.

[MALK07] Malkin, S.; Guo, C.: Thermal Analysis of Grinding. In: CIRP Annals, Vol. 56, 2007, pp. 760–782.

[MALK08] Malkin, S.; Guo, C.: Grinding Technology - Theory and Applications of Machining with Abrasives. Industrial Press, New York, 2008.

[MARI12] Marinescu, I. D.; Rowe, W. B.; Dimitrov, B.; Ohmori, H.: Tribology of Abrasive Machining Processes. Elsevier, Amsterdam, 2012.

[MARI15] Marinescu, I. D.; Doi, T. K.; Uhlmann, E.: Handbook of Ceramics Grinding and Polishing. Elsevier, Amsterdam, 2015.

[MATS13] Matsuda, T.; Matsubara, H.: Thermophysical and elastic properties of titanium carbonitrides containing molybdenum and tungsten. In: Journal of Alloys and Compounds, Vol. 562, 2013, pp. 90–94.

[MAZH20] Mazhnik, E.; Oganov, A. R.: Application of machine learning methods for predicting new superhard materials. In: Journal of Applied Physics, Vol. 128, 2020, pp. 1–14.

[MEMS92] MEMSnet: Material: Titanium Nitride (TiN), bulk, 1992. URL: https://www.memsnet.org/material/titaniumnitridetinbulk/.

[MOCH12] Mochalin, V. N.; Shenderova, O.; Ho, D.; Gogotsi, Y.: The properties and applications of nanodiamonds. In: Nature Nanotechnology, Vol. 7, 2012, pp. 11–23.

[MORG98] Morgan, M. N.; Rowe, W. B.; Black, S. C.: Effective thermal properties of grinding wheels and grains. In: Proceedings of the intitution of Mechanical Engineers, Vol. 212 Part B, 1998, pp. 661–669.

[MULL21] Müller, U.; Kaiser, J.; Barth, S.; Bergs, T.: The tribology between monocrystalline diamond and polycrystalline cubic boron nitride during frictional contact. In: Journal of Manufacturing Processes, Vol. 68, 2021, pp. 1147–1157.

[OKAB00] Okabe, A.; Boots, B.; Sugihara, K.; Sung Nok, C.: Spatial Tessellation: concepts and applications of Voronoi diagrams. John Wiley & Sons, New York, 2000.

[PIER99] Pierson, H. O.: Handbook of chemical vapor deposition. Noyes Publications, New York, 1999.

[POPO10] Popov, V. L.: Contact Mechanics and Friction. Springer, Berlin, 2010.

[PROE18] Proes, F.; Eichenseer, C.; Hintze, W. et al.: In situ analysis of PCBN cutting tool materials during thermo-mechanical loading using synchrotron radiation. In: Production Engineering Research and Development, Vol. 12, 2018, pp. 535–546.

[PROE18] Proes, F.; Eichenseer, C.; Hintze, W. et al.: In situ analysis of PCBN cutting tool materials during thermo-mechanical loading using synchrotron radiation. In: Production Engineering Research and Development, Vol. 12, 2018, pp. 535–546.

[QUES09] Quested, P. N.; Brooks, R. F.; Chapman, L. et al.: Measurement and estimation of thermophysical properties of nickel-based superalloys. In: Materials Science and Technology, Vol. 25, 2009, pp. 154–162.

[RASM83] Rasmussen, J.: Skills, rules, and knowledge; signals, signs, and symbols, and other distinctions in human performance models. In: IEEE Transactions on Systems, Man, and Cybernetics, Vol. SMC-13, 1983, pp. 257–266.

[RENT09] Rentsch, R.: Nanoscale cutting. In: J. P. Davim, M. J. Jackson (Eds.): Nano and micromachining. New Jersey, John Wiley & Sons, pp. 1–26.

[RENT14] Rentsch, R.: Molecular Dynamics for Cutting Processes. In: L. Laperrière, G. Reinhart (Eds.): CIRP Encyclopedia of Production Engineering. Berlin, Springer, pp. 897–901.

[ROWE14] Rowe, W. B.: Principles of Modern Grinding Technology. Elsevier, Amsterdam, 2014.

[SAFT20] Säfsten, K.; Elgh, F. (Eds.): SPS2020 - Proceedings of the Swedish Production Symposium.

[SAND21] Sandvik Coromant: Cutting tool materials, 2021. URL: https://www.sandvik.coromant.com/en-gb/knowledge/materials/pages/cutting-tool-materials.aspx.

[SCHI15] Schindler, F.: Zerspanungsmechanismen beim Schleifen von polykristallinem Diamant. Dissertation, RWTH Aachen, 2015.

[SLIP20] Slipchenko, K.; Stratiichuk, D.; Belyavina, N. et al.: Evolution of the Microstructure and Mechanical Properties of cBN-Based Cutting Tools with Silicides Compounds as Binder Phase. In: Proceedings of the Swedish Production Symposium. Sweden, 7th - 8th October 2020. Amsterdam, IOS Press, pp. 428–438.

[SOLO91] Solozhenko, V. L.: The thermodynamic aspect of boron nitride polymorphism and the BN phase diagram. In: High Pressure Research, Vol. 7, 1991, pp. 201–203.

[SOO16] Soo, S. L.; Khan, S.A.; Aspinwall, D. K. et al.: High-speed turning of Inconel 718 using PVD-coated PCBN tools. In: CIRP Annals, Vol. 65, 2016, pp. 89–92.

[SPRO96] Sproul, W. D.: New Routes in the Preparation of Mechanically Hard Films. In: Science, Vol. 273, 1996, pp. 889–892.

[SUMI19] Sumitomo Electric Carbide Inc.: New Binderless CBN & PCD Turning Grades, 2019. URL: https://sumicarbide.com/new-innovations/#tab-content2.

[SUMI16] Sumiya, H.; Harano, K.: Innovative Ultra-hard Materials: Binderless Nano-polycrystalline Diamond and Nano-polycrystalline Cubic Boron Nitride. In: SEI Technical review, Vol. 82, 2016, pp. 21–26.

[SUMI14] Sumiya, H.; Harano, K.; Ishida, Y.: Mechanical properties of nano-polycrystalline cBN synthesized by direct conversion sintering under HPHT. In: Diamond and Related Materials, Vol. 41, 2014, pp. 14–19.

[SUMI96] Sumiya, H.; Satoh, S.: High-pressure synthesis of high-purity diamond crystal. In: Diamond and Related Materials, Vol. 5, 1996, pp. 1359–1365.

[TAN90] Tan, H.; Ahrens, T. J.: Shock induced polymorphic transition in quartz, carbon, and boron nitride. In: Journal of Applied Physics, Vol. 67, 1990, pp. 217–224.

[TANA16] Tanaka, H.; Sugihara, T.; Enomoto, T.: High Speed Machining of Inconel 718 Focusing on Wear Behaviors of PCBN Cutting Tool. In: Procedia CIRP, Vol. 46, 2016, pp. 545–548.

[TAY18] Tay, B. K.; Bodelot, L.; Lebental, B. et al. (Eds.): 2018 IEEE 8th International Nanoelectronics Conferences.

[TEKK14] Tekkaya, A.E.; Soyarslan, C.: Finite Element Method. In: L. Laperrière, G. Reinhart (Eds.): CIRP Encyclopedia of Production Engineering. Berlin, Springer, pp. 508–514.

[TYAG17] Tyagi, A.K.; Banerjee, S. (Eds.): Materials Under Extreme Conditions: Recent Trends and Future Prospects. Elsevier, Netherlands, 2017.

[VEL91] Vel, L.; Demazeau, G.; Etourneau, J.: Cubic boron nitride: synthesis, physicochemical properties and applications. In: Materials Science and Engineering, Vol. 10, 1991, pp. 149–164.

[VEPR99] Veprek, S.: The search for novel, superhard materials. In: Journal of Vacuum Science & Technology A, Vol. 70, 1999, pp. 691–697.

[VEPR16] Veprek, S.; Veprek-Heijman, M.G.J.: Superhard and Ultrahard Nanostructures Materials and Coatings. In: V. Kanyanta (Ed.): Microstructure-Property Correlations for Hard, Superhard, and Ultrahard Materials. Cham, Springer, pp. 167–210.

[VITS20] Vits, F. J.: Tribologie beim Schleifen von polykristallinem Diamant. Dissertation, RWTH Aachen, 2020.

[WANG05] Wang, Z. G.; Wong, Y. S.; Rahman, M.: High-speed milling of titanium alloys using binderless CBN tools. In: International Journal of Machine Tools and Manufacture, Vol. 45, 2005, pp. 105–114.

[WENT57] Wentorf, R. H.: Cubic Form of Boron Nitride. In: The Journal of Chemical Physics, Vol. 26, 1957, pp. 956.

[WENT61a] Property right US 2996763-A (22.08.1961). Wentorf, R. H.: Diamond material.

[WENT61b] Property right GB 860499-A (08.02.1961). Wentorf, R. H.: Methods of making cubic boron nitride.

[WENT80] Wentorf, R. H.; De Vries, R.C.; Bundy, F. P.: Sintered Superhard Materials. In: Science, Vol. 208, 1980, pp. 873–880.

[XU15] Xu, B.; Tian, Y.: Superhard materials: recent research progress and prospects. In: Science China Materials, Vol. 58, 2015, pp. 132–142.

[YAN18] Yan, X.; Li, X.; Wang, X. et al.: Microstructural features and thermal stability of alumina-bonded nano-polycrystalline diamond synthesized by detonation sintering. In: Ceramics International, Vol. 44, 2018, pp. 22045–22052.

[YAN09] Yan, X.; Su, X.: Linear regression analysis. World Scientific, Singapore, 2009.

[YAO16] Yao, Q.; Shang, S.; Hu, Y. et al.: First-principles investigation of phase stability, elastic and thermodynamic properties in L12 Co3(Al,Mo,Nb) phase. In: Intermetallics, Vol. 78, 2016, pp. 1–7.

[ZHAO07] Zhao, Y. C.; Wang, M. Z.: Cubic BN Sintered with Al under High Temperature and High Pressure. In: Chinese Physics Letters. Chinese Physical Society, Vol. 24, 2007, pp. 2412–2414.